Impact of shallow sills on ~~heat transport and stratification~~ circulation regimes and submarine melting in ~~proglacial~~ glacial fjords

Weiyang Bao[1] and Carlos Moffat[1]

[1]School of Marine Science and Policy, University of Delaware, Newark, DE, USA

Correspondence: Weiyang Bao (wbao@udel.edu)

Abstract. The increased melting and rapid retreat of marine-terminating glaciers is a ~~main~~ key contributor to sea level rise. In ~~shallow-silled fjords~~ glacial fjords with shallow sills common in Patagonia, Alaska, and other systems, these bathymetric features ~~may act as the~~ can act as a first-order control on the dynamics~~, constraining fjord-shelf exchange and thereby modulating glacial melting~~. However, ~~we still lack a clear~~ our understanding of how ~~circulation and associated heat transport in shallow-silled glacial fjords are modulated by fjord-glacier geometry and fjord-shelf properties~~ this shallow bathymetry interacts with the subglacial discharge from the glacier and impacts the fjord circulation, water properties, and rates of submarine melting is limited. To address this ~~,~~ gap, we conduct idealized numerical simulations ~~are conducted~~ using a coupled plume-ocean fjord model ~~. The steady-state fjord exhibits~~ spanning a wide range of initial ocean conditions, sill depths, and subglacial discharge. A previously documented circulation regime leads to strong mixing and vertical transport over the sill~~.~~ ~~Relatively~~, where up to ~70% of the colder water from the upper-layer outflow is refluxed into the deeper layer, cooling the incoming warm oceanic water ~~and modifying water properties~~ by as much as $1°C$ and reducing the stratification near the glacier front. ~~Driven by a shallow sill, up to ~70% of the outflow is refluxed downward and leads to ~10% cooling of the inflow and the deep fjord. A range of sensitivity experiments indicate that sill depth, subglacial discharge, ambient fjord temperature and stratification are key parameters that modulate the heat transport to the glacier terminus. In particular, the relative depth of~~ When the initial stratification is relatively strong or the subglacial discharge is relatively weak, an additional unsteady circulation regime arises where the freshwater flow can become trapped below the sill depth for weeks to months, creating an effective cooling mechanism for the deep water. We also find that submarine melting often increases when a shallow sill is added to a glacial fjord due to the reduction of stratification–which increases submarine melting–dominating over the cooling effect as the oceanic inflow is modified by the presence of the ~~fjord, the sill, and the terminal height of meltwater plume are used to characterize four circulation and heat transport regimes. The sill-driven reflux is found to result in a decrease of both deep fjord temperature and stratification, which have opposite effects on the glacial melt rate~~ sill. These results underscore ~~the importance of sill bathymetry and associated fjord processes in the variability of oceanic heat supply to melting~~ that shallow-silled fjords can have distinct dynamics that strongly modulate oceanic properties and the melting rates of marine-terminating glaciers.

1 Introduction

From 2000 to 2019, global glaciers ~~have~~ lost mass at a rate of $\sim 267\ Gt\,yr^{-1}$, which amounts to approximately twenty percent of the observed sea-level rise (Hugonnet et al., 2021). As a critical link between glaciers, ice sheets, and the large-scale ocean, glacial fjords and their dynamics modulate the retreat rates of glaciers and the offshore transport of freshwater discharge. Increased submarine melting of glaciers terminating in fjords ~~is the main cause for~~ can be a significant contributor to glacier retreat, and the resulting freshwater is transformed by fjord processes before being released to the ocean (Straneo and Cenedese, 2015). Knowledge of fjord dynamics and processes is thus key to estimating glacier melt rates and ~~for~~ understanding the fate of ~~the~~ meltwater in the coastal ocean.

At the fjord scale, the circulation can be influenced by tides, local winds and other air-sea exchange processes, and interactions of buoyancy-driven and intermediary flows (Straneo and Cenedese, 2015). At the glacier front, buoyant plumes generated by subglacial discharge and/or submarine melting are a source of mass and freshwater for the system (e.g., Xu et al., 2013; Kimura et al., 2014). The resulting buoyancy-driven circulation results from this freshwater, leaving the terminus and mixing with ambient water, the latter being replaced by a deep inflow towards the fjord head. The intermediary circulation driven by variability outside the fjord, on the other hand, is an effective mechanism for the advection of shelf anomalies inside the fjord, is often stronger than the estuarine-like circulation, and likely has an impact on melting rates (Sciascia et al., 2014; Moffat, 2014; Jackson et al., 2014). However, our estimates of submarine melt rates are still highly uncertain ~~because of~~ due to limited observations and ~~model accuracy~~ potential shortcomings in existing parameterizations (Jackson et al., 2020).

A key control on the circulation of fjord systems is the presence of a shallow sill (Geyer and Cannon, 1982; Arneborg et al., 2004; Inall et al., 2004). While many studies have focused on large ~~fjord systems with no deep or no~~ fjords with no or deep sill (Sutherland et al., 2014; Bartholomaus et al., 2016; Rignot et al., 2016), shallow sills are common in fjords in Alaska, Patagonia, and Greenland where the widespread retreat of glaciers is impacting sea-level rise and ~~the~~ regional ecosystems (Mortensen et al., 2013; Motyka et al., 2013; Moffat et al., 2018). In southeastern Greenland, Sutherland et al. (2014) investigated the circulation regimes of two major outlet glacial fjords and found that the magnitudes of the estuarine and intermediary circulation are determined by the sill depth compared to the fjord depth, with shallower sills corresponding to weaker intermediary circulation. ~~In-situ observations collected in front of the floating tongue of a Greenland glacier also indicate the interface height between warm oceanic inflow and colder overlying water above the sill modulates the temporal variability of ocean heat transport through hydraulic control, with a higher interface enhancing the cavity overturning circulation and the heat supplied for glacier melting (Schaffer et al., 2020).~~

Numerical simulation studies have also emphasized the importance of geometric parameters in controlling fjord renewal and exchange. Idealized modeling with varying depths of subglacial discharge in sill fjords shows that the depth of the grounding line compared to the sill is a primary control on the plume-driven renewal of basin waters (Carroll et al., 2017). When the ~~inflow~~ inflow is deeper than the sill, ~~it is the former that~~ the former determines the depth of the exchange circulation. For subglacial discharge entering at the grounding line of a glacier with a sill shallower than the terminus, the exchange flow spans the entire water column (Carroll et al., 2017). ~~Besides~~In addition, Zhao et al. (2021) addressed geometric and forcing

parameters that control the fjord-to-shelf overturning circulation by ~~piecing together~~ combining theories for transport across the continental shelf, the fjord mouth sill, and the fjord head. Their numerical experiments demonstrated sill depth as one of the first-order controllers on the overturning circulation~~and a functional prediction between the controlling parameters and the overturning transport was developed~~. Most recently, a study in LeConte Bay, Alaska based on both numerical modeling and observations~~showed that the deep ,~~, showed that deep incoming flow can be ~~cooled significantly~~ significantly cooled at the sill by mixing with the outgoing freshwater outflow, a process called reflux (Hager et al., 2022). And while not the focus of this study, even deep sills can play a key role in modulating deep water properties and the heat supply to marine-terminating glaciers (Schaffer et al., 2020; Nilsson et al., 2023). All of these studies highlight that the mass and heat exchange ~~process in fjords with shallow sills~~ processes in fjords are significantly different ~~from their deep-silled counterparts~~when a sill is present.

We aim to understand how ~~the dynamics of shallow-silled fjords modulate the heat exchange and transport towards marine-terminating glaciers~~shallow sills modulate the water properties, circulation, and rates of submarine melting in glacial fjords. We use idealized numerical simulations based on a coupled plume-ocean model ~~to investigate the constraining effects of the sill on the transport of heat from the open ocean to the glacier terminus, considering a broad range of fjord and forcing characteristics~~setup to explore a range of sill depths, shelf properties, and glacial forcing. We also aim to extend the results of Hager et al. (2022) for LeConte Bay to understand the role of reflux when different sill depths and forcing conditions are considered. Because freshwater discharge and ocean conditions in these systems often vary significantly in seasonal scales, ~~we aim~~ our objective is to understand the circulation in ~~that or shorter time-scales. We set up our simulations to examine, in particular, the role of varying the sill depth, stratification, and freshwater discharge on heat transport and submarine melt rates.~~ those or shorter timescales. Our model setup is introduced in ~~section~~ Section 2, followed by results in ~~section~~ Section 3, and discussion and conclusions in ~~sections~~ Sections 4 and 5, respectively.

2 Methodology

2.1 Coupled Plume-Ocean Fjord Model

We use the Massachusetts Institute of Technology General Circulation Model ~~(MITgem)~~ (MITgcm; Marshall et al., 1997) in a three-dimensional ~~,~~hydrostatic configuration. ~~MITgem (Marshall et al., 1997) includes options to incorporate horizontal~~ The model can incorporate ice shelves and vertical ice faces ~~,~~and has been used in several studies of ice-ocean interactions ~~both beneath ice shelves and~~ in glacial fjords ~~(Losch, 2008; Xu et al., 2012)~~(e.g., Xu et al., 2012; Carroll et al., 2016; Hager et al., 2022). Since the fjord-scale model lacks the grid resolution to resolve ~~non-hydrostatic plume~~ the small-scale dynamics at the ice front, ~~a theoretical plume model (Morton et al., 1956) is embedded as an MITgem module in order to parameterize vertical convection in a half-conical, point source vertical~~ we use the IcePlume package (Cowton et al., 2015) to parameterize the formation of a buoyant plume adjacent to the glacier terminus ~~(Cowton et al., 2015). The submarine melt rate is calculated based on the plume temperature, salinity, and velocity, as well as the ice-ocean boundary layer temperature and salinity (Holland and Jenkins, 1999). In our simulations, the freshwater input from submarine melting is parameterized as a virtual~~

~~salt flux, generating a very small (< 1%) increase in the exchange-flow transport and negligible freshening and cooling of fjord waters compared to that from subglacial discharge~~and obtain estimates of the resulting submarine melt.

The ~~model uses a vertical glacier terminus grounded to the fjord bottom, where subglacial runoff is specified and ambient conditions from the ocean are passed to the plume module at each time step. The module~~ IcePlume package implements the evolution of a plume for a given buoyancy forcing, ~~stratification~~ stratification, and geometry from ~~an~~ idealized plume theory (Morton et al., 1956). Simplified expressions for ~~the plume properties can be derived following the assumption~~ plume properties are derived assuming that the entrainment velocity is a fixed fraction of the vertical velocity in the plume. The plume radius, velocity, temperature, salinity, and vertical extent are calculated, with the plume ascent terminating when it reaches neutral buoyancy (i.e., the plume density is equal to the ambient density) or the fjord surface. Water, heat, and salt are then removed from MITgcm cells in ~~those vertical layers where the plume is entraining~~which ambient water is being entrained into the ascending plume, and put into the cell at the depth at which the plume ~~is predicted to terminate (Cowton et al., 2015). The plume model is run at each timestep using the current conditions within the fjord, with a steady-state solution calculated and applied as boundary conditions to the coarser fjord domain. This coupled model has the advantage of permitting a relatively coarse spatial and temporal resolution to be used throughout the domain, greatly increasing computational efficiency.~~

~~We emphasize, however, that the dynamical response of the submerged glacier terminus to ocean forcing is complex. Studies have shown, for example, that the formation of cavities in the ice that can significantly change the rates of submarine melting, driving higher than predicted melting (Jackson et al., 2017). While that complexity is not well represented in our simplified melting model,~~ terminates, that is, stops ascending (Cowton et al., 2015). In grid locations where subglacial discharge is specified, the submarine melt rate is calculated based on the temperature, salinity, and velocity of the ~~qualitative change in melting rates from simplified models is still a useful guide for understanding how the geometry of the fjord and the forcing conditions impact heat transport and~~ plume, as well as the ice-ocean boundary layer temperature and salinity (Holland and Jenkins, 1999). In the grid cells along the remainder of the glacier front, the ~~circulation of the fjord~~melt rate is obtained using the temperature, salinity, and velocity from the adjacent MITgcm cells. The resulting submarine melting is then incorporated as virtual salt and heat fluxes to those adjacent grid cells. Relative to the cooling and freshening caused by the subglacial discharge, the melting generates a relatively small freshwater input (Cowton et al., 2015).

To investigate the response of fjord circulation and submarine melting to variations in forcing and fjord geometry, we set up the plume-ocean fjord model in a domain with one Gaussian-shaped sill near the mouth (Fig. 1). The sill has a fixed width of $4\ km$ and a ~~maximum~~ shallowest depth of h_s, which is varied in our simulations to examine the role of sill depth in modulating fjord circulation and heat supply to the glacier. The fjord domain is set to $2\ km$ wide to limit the scope of our study to a reasonable set of parameters. While relatively narrow, we will show that this does not prevent the generation of significant cross-fjord variability in the circulation. The maximum depth of h_f is $400\ m$ in ~~all simulations~~most cases, with a handful of cases using $200\ m$ to test our results in a broader parameter space. The fjord is $20\ km$ long and opens to a shelf region (~~25~~27 km ~~wide~~long, $16\ km$ wide, and $400\ m$ deep), with open boundaries at the north, south, and east edges. The cross-fjord grid resolution is $200\ m$ inside the fjord, linearly increasing to $1\ km$ at open boundaries. The along-fjord grid resolution ranges
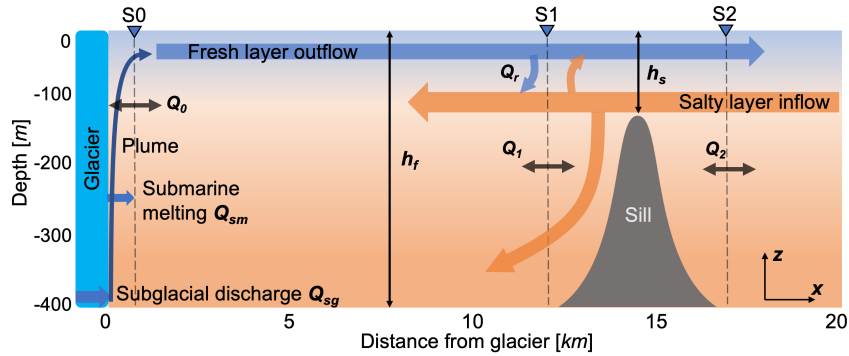
Figure 1. Two-dimensional ~~view~~ schematic (x, z) ~~view of fjord domain and~~ the ~~plume-driven exchange flow~~ circulation and water properties in a glacial fjord. The ~~maximum sill depth and~~ flow in a fjord of depth ~~are denoted~~ h_f is constrained by a sill of depth h_s ~~and h_f respectively, dashed lines represent cross-fjord sections~~. Cross-sections for analysis are defined near the glacier front (S0) and ~~at~~ on either side of the sill (S1, S2). ~~H, Q~~ Q_0, Q_1, Q_2 are ~~heat and~~ volume fluxes through the sections and in the vertical (~~H_r, Q_r~~ Q_v).

125 from 20 m at the sill to 100 m at the rest of the fjord, also linearly telescoping to 1 km at open boundaries. ~~Vertical~~ The vertical grid size of the ~~entire~~ model domain increases from 2 m at the free surface to 6 m at the bottom.

~~Initial~~ The variables changed for different runs (geometry as well as initial and forcing conditions) are listed in Table 1. The initial fjord conditions are horizontally homogeneous. ~~Initial~~, with temperature and salinity profiles restored at open boundaries on the shelf throughout the simulation. We changed the size of the shelf and found no significant difference in

130 our results, suggesting that they are not impacted by these boundary conditions. The initial water temperature is a constant ~~of~~ ranging from 2 to 10 $^\circ C$. ~~The vertical salinity gradient is based on an idealized~~ Most runs used an idealized initial salinity based on a Greenland fjord profile (Cowton et al., 2015), where the salinity ranges from 32 to 33.8 ~~at the surface~~ in the upper 80 m and slowly increases to 34.5 at the bottom ~~. To explore the impacts of fjord~~ ("Idealized" in Table 1). To further explore the impact of varying stratification, we also set up a set of experiments with a ~~simplified salinity profile linearly increasing~~ linear

135 salinity profile that increases from 23 ~~at~~ on the surface to 27 at the bottom with a stratification of $7.36 \times 10^{-5} \ s^{-2}$ defined as $1N_0^2$. With a fixed mid-depth salinity, the gradient and thus the initial ambient stratification ~~ranges~~ range from $0.5N_0^2$ to $4N_0^2$. Initial velocities are zero throughout the domain except for tidal simulations. For runs that include tidal forcing, ~~this forcing~~ a uniform zonal velocity is applied along the eastern boundary (the fjord is oriented east-west) of the model domain ~~in the form of a uniform zonal velocity $U_t = U_0 \sin(\frac{2\pi}{T} t)$ at the M2~~ $U_t = U_0 \sin(\omega t)$ at the M_2 tidal period (~~$T=12.42$ hr~~), $\omega = 2\pi/12.42 h$;

140 t is time), where the velocity amplitude U_0 ~~is set to different values~~ ranges from 0.01 to 6 $cm \ s^{-1}$ to generate weak ~~and strong tidal currents in the fjord~~ to strong tides relative to the ~~non-tidal exchange flow~~ subtidal exchange flow at the sill. The Coriolis parameter is set to ~~1.2×10^{-4}. The nonlocal~~ $1.2 \times 10^{-4} \ s^{-1}$. The K-Profile Parameterization (KPP) scheme (Large et al., 1994) is used ~~for~~ to parameterize vertical mixing. A quadratic bottom drag parameterization ~~was used. The drag coefficient was~~ with a drag coefficient of 2.5×10^{-3} for most ~~simulations~~ runs, but we conducted a small set of simulations using a range

145 ~~1~25~~1-25 $\times 10^{-3}$ to test the impact of varying bottom drag. Those runs are not shown, but changing the drag coefficient did not meaningfully impact our results.

We ~~also utilize~~ used passive tracers (MITgcm PTRACERS package) to estimate the timescales of the response of the fjord to changes in shelf properties. For this purpose, a first tracer with a constant concentration ~~of one~~ was introduced at the entire shelf region, ~~meanwhile~~ and a second tracer ~~is~~ was injected into the same region ~~with the same boundary conditions~~ but its

150 concentration increases with time at a fixed rate. Then the ratio of these two tracers in any model grid is used to estimate the ~~"age"~~ 'age' of the shelf water tracer at that location (e.g., Rayson et al., 2016; MacCready et al., 2021).

We ~~analysed 73 model runs with a variety of parameters, including sill depth~~ emphasize, however, that both the dynamics of the fjord circulation and the dynamical response of the submerged glacier terminus to ocean forcing are complex. Studies have shown, for example, that the formation of cavities in the ice can significantly change the rates of submarine melting, driving

155 higher than predicted melting (Jackson et al., 2017) and that existing melting parameterizations underestimate the observed background melting rates (Jackson et al., 2020). Our choice of simplified sill is meant to understand the role of bathymetric constrictions on the flow, including enhanced mixing. In real fjord systems, enhanced mixing could also be promoted by other bathymetric features, multiple sills, icebergs (Hager et al., 2023), or other factors. This complexity is not well represented in our simplified model, but our setup is still a useful guide to exploring the dynamics of ice-ocean interactions in systems with

160 shallow sills.

We analyzed 93 model runs where we varied the sill depth h_s, subglacial discharge Q_{sg}, initial fjord temperature T_{ini}, stratification N_{ini}^2, bottom drag C_d, and tidal forcing (Table 1). The ~~maximum~~ shallowest sill depth h_s is nondimensionalized by dividing by the maximum fjord depth h_f, and this depth ratio h_s/h_f varies from 0.04 to 0.12 to characterize shallow-silled fjord systems, e.g., in Alaska (Motyka et al., 2013; Love et al., 2016) and Patagonia (Moffat et al., 2018). Cases ~~with~~

165 ~~no~~ without sill ($h_s/h_f = 1$) are included ~~for reference~~ to understand the overall impact of the sill. The subglacial discharge flux Q_{sg} is varied in the range 25 to 1000 $m^3 s^{-1}$ to cover different magnitudes of freshwater forcing ~~,~~ and to represent the seasonal variation of runoff, although we recognize that the high end of this range is likely unrealistic given the size of our domain. All simulations are run for 60 days, in which ~~the fjord circulation reached a steady state~~ ~~for most cases~~ most runs reached a near-steady state, where key aspects of the circulation (e.g., exchange flow) and water properties (layer thicknesses,

170 heat storage) did not change meaningfully with time.

2.2 Total Exchange Flow and Efflux-Reflux Calculations

The exchange flow along the fjord is calculated using the total exchange flow (TEF) method (MacCready, 2011). Transports through a cross-fjord section are sorted into salinity classes, tidally averaged and then integrated vertically and across the fjord. The inflow volume flux Q_{in} is the sum of the transport in all ~~inward flowing~~ inward-flowing salinity classes, and the flux-

175 weighted salinity of the inflow is S_{in}. Similarly, the outflow is quantified as Q_{out} and S_{out}. The TEF method decomposes salt flux in salinity space instead of physical space, yielding the exchange flow that incorporates both tidal and subtidal processes ~~,~~ and satisfies the Knudsen relation precisely (MacCready, 2011). TEF has been ~~applied in many estuarine systems and has the ability to clearly characterize the exchange flow (Geyer and MacCready, 2014; Wang et al., 2017; MacCready et al., 2021)~~

Table 1. ~~List~~ Summary of fjord ~~parameters~~ geometry, initial conditions, and ~~corresponding cases for simulations~~ forcing conditions used in 93 model runs analyzed. h_s: maximum sill depth, h_f: maximum fjord depth, Q_{sg}: subglacial discharge, T_{ini}: initial fjord temperature, N_{ini}^2: initial fjord stratification, C_d: quadratic bottom friction coefficient, U_0: tidal amplitude at the eastern open boundary. The linear stratification profile corresponds to values ranging from 0.5 to 4 $\times N_0^2$ ($N_0^2 = 7.36 \times 10^{-5}\ s^{-2}$).

h_s/h_f	~~h~~h_f (m)	$Q_{sg}\ (m^3\,s^{-1})$	$T_{ini}\ (^{\circ}C)$	$N_{ini}^2\ (s^{-2})$	$C_d\ (\times 10^{-3})$	$U_0\ (cm\,s^{-1})$	# of Runs
0.04, 0.06, 0.08, 0.1, 0.12, 1	400	250	10	~~non-linear~~ Idealized	2.5	0	6
0.04, 0.12, 1	400	25, 50, 100, 500, 1000	10	~~non-linear~~ Idealized	2.5	0	15
0.04, 0.12, 1	200	25, 50, 100, 250, 500, 1000	10	~~non-linear~~ Idealized	2.5	0	18
0.08	400	50, 500	2, 4, 6, 8	~~non-linear~~ Idealized	2.5	0	8
0.04, 1	400	250	2, 6, 10	~~$0.5N_0^2, 1N_0^2, 2N_0^2, 3N_0^2, 4N_0^2$~~ Linear	2.5	0	~~10~~ 30
0.04, 0.12	400	250	10	~~non-linear~~ Idealized	1, 10, 25	0	6
0.04, 0.12	400	250	10	~~non-linear~~ Idealized	2.5	0.01, 0.1, 0.5, 1, 6	10

180 ~~. In our idealized fjord system presumably but not necessarily dominated by a two-layer circulation, using~~ used extensively in estuarine systems (Geyer and MacCready, 2014; Wang et al., 2017; MacCready et al., 2021).

To apply the TEF method ~~gives the total inflow and outflow fluxes through a cross-fjord section regardless of they are associated with exchange flow or tidal pumping.~~

~~The~~, the volume transport through each cross-section is binned with salinity output stored every six hours, using 1000 bins between 0 and 35. After tidally averaging (for runs where tides are included), the transport at each time is divided into

185 inflowing and outflowing components according to the ~~"dividing salinity "~~ dividing salinity method (MacCready et al., 2018). Integrating ~~the transport in either landward or seaward~~ transport in glacierward or oceanward components gives us Q_{in} and Q_{out}. Similarly, integrating the transport times the salinity of each bin in the two directions gives the ~~in- and outflow~~ inflowing and outflowing salt flux. Then S_{in} and S_{out} are derived from dividing the salt flux by the volume flux in the same direction. Based on steady-state volume conservation, the entrainment flux (downward reflux) Q_r across the upper-bounding isohaline

190 surface equals the divergence of inflow or outflow through the segment bonded by two cross-sections (Wang et al., 2017).

~~In order to~~ To estimate and quantify the vertical exchange between the upper and lower layers, we utilize the efflux-reflux formalism that was first developed in Cokelet and Stewart (1985) and has been applied to both estuary and glacial fjord studies ~~(MacCready et al., 2021; Hager et al., 2022)~~ (MacCready et al., 2021; Hager et al., 2022, 2023). In its simplest form, the efflux-reflux theory defines a channel segment between two cross-fjord sections ~~. The segment consists of~~ with a steady

195 two-layer exchange flow ~~, with~~ and known salt and volume transports through the cross-sections on either side (Fig. 2a). For the flow from any incoming layer, the reflux fraction corresponds to independent upward and downward turbulent transports across the segment, while efflux is the fraction that continues moving into the next reach. The reflux fraction ~~thereby~~ therefore expresses the vertical fluxes as volume transports, which is equivalent to the horizontal fluxes in TEF. All transports are positive, the two cross-sections (S1 and S2) connect three segments, each of which has two layers in the vertical, a shallow fresher

200 one and a deep saltier one. Following Cokelet and Stewart (1985), the system of equations to be solved ~~may be written as~~ is:
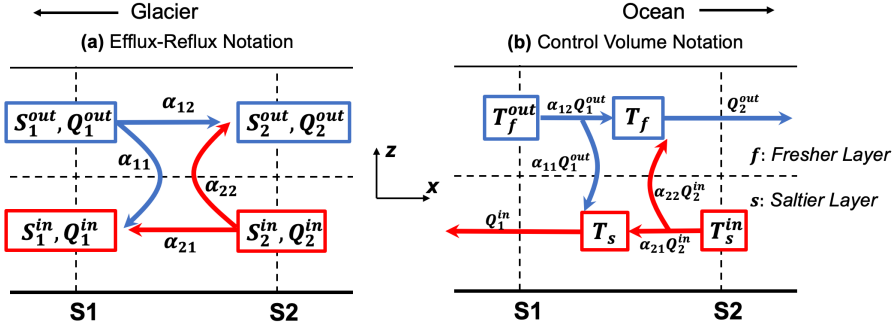
Figure 2. Notations of (a) efflux-reflux calculation and (b) a control volume. The segment ~~in~~ between sections S1 and S2 has a fresher layer and a saltier layer in the vertical. Temperature, salinity, and volume fluxes are denoted by T, S, and Q. $\alpha_{from,to}$ represent the efflux-reflux fractions. Figure modified from Fig. 7 in MacCready et al. (2021).

$$
\begin{bmatrix}
Q_2^{in} & Q_1^{out} & 0 & 0 \\
S_2^{in}Q_2^{in} & S_1^{out}Q_1^{out} & 0 & 0 \\
0 & 0 & Q_2^{in} & Q_1^{out} \\
0 & 0 & S_2^{in}Q_2^{in} & S_1^{out}Q_1^{out}
\end{bmatrix}
\begin{bmatrix}
\alpha_{22} \\
\alpha_{12} \\
\alpha_{21} \\
\alpha_{11}
\end{bmatrix}
=
\begin{bmatrix}
Q_2^{out} \\
S_2^{out}Q_2^{out} \\
Q_1^{in} \\
S_1^{out}Q_1^{out}
\end{bmatrix}
\tag{1}
$$

The efflux-reflux coefficients α are then determined by solving the matrix equation based on the conservation of volume and salt, and the sum of efflux and reflux fractions should be equal to unity, ~~i.e.~~that is, $\alpha_{11} + \alpha_{12} = \alpha_{21} + \alpha_{22} = 1$. In this framework, the vertical exchange components that we are primarily concerned with can be solved as ~~:~~

205
$$
\alpha_{11} = \frac{Q_1^{out}}{Q_1^{in}}\frac{S_2^{in}-S_1^{out}}{S_2^{in}-S_1^{in}}\frac{Q_1^{in}}{Q_1^{out}}\frac{S_2^{in}-S_1^{in}}{S_2^{in}-S_1^{out}}, \; \alpha_{22} = \frac{Q_2^{out}}{Q_2^{in}}\frac{S_2^{out}-S_1^{in}}{S_2^{in}-S_1^{in}}\frac{Q_2^{out}}{Q_2^{in}}\frac{S_2^{out}-S_1^{out}}{S_2^{in}-S_1^{out}}
\tag{2}
$$

Combining efflux-reflux fractions and TEF transports, a control volume can be defined for layer temperature along the fjord (Fig. 2b). It is also bounded by two cross-fjord sections S1 and S2, ~~the free sea surface, sidewalls and the fjord bottom~~with no exchange at the sea surface. A third section (S0) is defined to understand the near-glacier properties and circulation. The layer interface ~~in~~ throughout the control volume is determined by the zero-crossing point of the along-channel velocity profile,

210 ~~an approximation of the exchangeflow structure~~which assumes a two-layer exchange. Following the notation in Fig. 2b, the equation for the temperature of the lower (saltier) layer with a volume of V_s can be expressed as:

$$
\frac{\mathrm{d}T_s}{\mathrm{d}t}V_s = T_s^{in}Q_2^{in}(1-\alpha_{22}) + T_fQ_1^{in\,out}\alpha_{11} - T_sQ_1^{out\,in}
\tag{3}
$$

At steady state ($\frac{\mathrm{d}T_s}{\mathrm{d}t}=0$ ~~dT_s/dt = 0~~), the expression of the lower layer temperature becomes

$$T_s = \frac{T_s^{in}Q_2^{in}(1-\alpha_{22}) + T_f Q_1^{in}\alpha_{11}}{Q_1^{out}} \frac{T_s^{in}Q_2^{in}(1-\alpha_{22}) + T_f Q_1^{out}\alpha_{11}}{Q_1^{in}} \tag{4}$$

As a result, we We can use the reflux part $(\alpha_{11}, \alpha_{22})$ of the efflux-reflux calculation to determine the vertical transport together with the TEF calculations to determine both horizontal and vertical transports and deep-layer temperature in the control volume. And to solve the matrix equation and obtain the efflux-reflux coefficients, we applied the TEF method at the cross-sections to get the salinity and transport (S As we will show later, the exchange flow at the sill might be of secondary importance to water modification and exchange occurring elsewhere, or the exchange flow might have three layers, and Q) of inflows and outflows. This approach quantifies the net effect of mixing and vertical exchange in the fjord without the need to resolve the process itself. To address the role of sill in modulating vertical transports and the heat supply to the glacier terminus, TEF transports, reflux coefficients and deep-layer temperature are estimated in the segment bonded by cross-fjord sections on either side of the sill (Fig. 1). Another cross-section is used to calculate the volume and heat fluxes near the glacier front. These segments are also defined to construct the volume and heat budgets within the fjord, following the framework in a generic glacial fjord study by Jackson and Straneo (2016). thus we are limiting the use of this approach only to cases where there is a well-defined two-layer exchange flow at the sill.

3 Results

3.1 Base Case: First-Order Impacts of a Shallow Sill

To illustrate the first-order impact of the sill on fjord-shelf exchange in our runs, we present a base case driven only by by thermal forcing and subglacial discharge in fjords under varying sill depths. A buoyant plume is generated by the fresh and cold subglacial runoff that enters the fjord at the glacier grounding line Q_{sg} is set to $250\ m^3 s^{-1}$, and drives the formation of a buoyant plume, entraining ambient warm water while rising vertically along the glacier front. With a fixed discharge of $250\ m^3 s^{-1}$, the plume drives a thin and cold down-fjord current in the upper part of the water column, This entrainment into the outflowing plume is balanced by a thick and warm up-fjord current at depth, and the return flow of warm oceanic water at depth. The fjord reached a steady state after in about a week. Runs with with varied We vary the sill-fjord depth ratios (i.e., h_s/h_f) ranging from 0.04 to 0.12 allowed to focus on the impact on to characterize the impact of shallow sills on the exchange of mass and heat mass exchange between the fjord and the shelf, and the cooling of deep oceanic water across the mouth of the fjord (Fig. 3).

As the sill depth increases, the layer thickness of the surface outflow initially remains between Increasingly shallow sills create strong mixing there, resulting in the cooling of the warm oceanic layer flowing toward the glacier. With no sill and the plume reaching the surface ($h_s/h_f = 1$, Fig. 3a), the outflow occupies the top 40 to 45 m of the water column in the fjord interior , but eventually decreases after reaching the sill with sill-fjord depth ratios <0.12. In these shallow sill cases, the lower-layer inflow cools by 0.2 to 1 and, as expected, the exchange between upper and lower layers, Q_r, is negligible. As
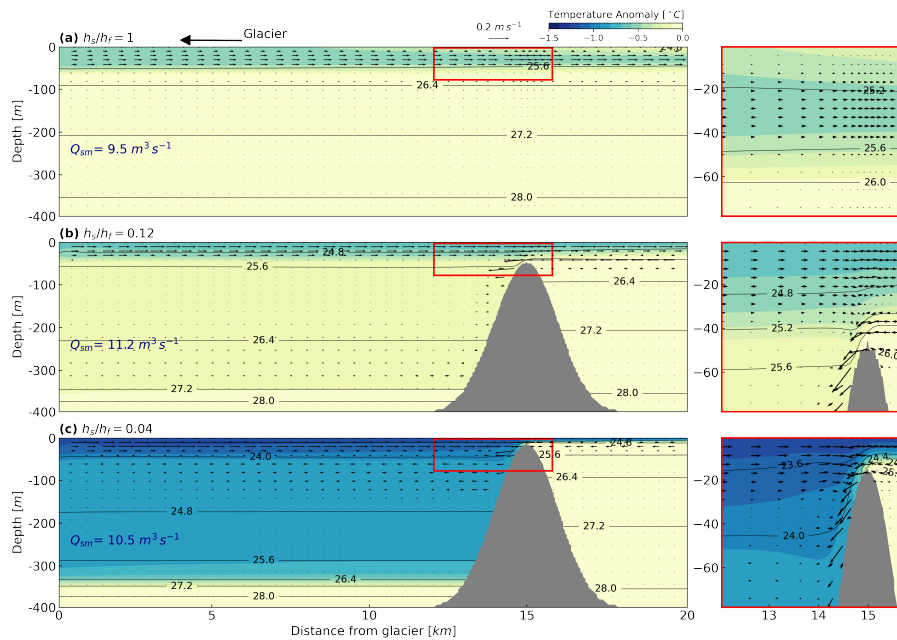
Figure 3. Time-mean (averaged over the last 14 days of simulations) potential temperature anomaly (with respect to an initial temperature of 10 °C)~~along the fjord with~~. All cases have $Q_{sg} = 250\ m^3 s^{-1}$ and sill depth varies from (a) $h_s/h_f = 1$, (b) $h_s/h_f = 0.12$, and (c) $h_s/h_f = 0.04$. ~~Red-outlined~~ The red-outlined areas are zoomed in on the right panels, with vertical velocity scaled up by a factor of 15. Black contours denote water density anomaly, Q_{sm} is ~~average~~ the volume flux of submarine melting~~of the glacier front~~.

the sill depth shallows ($h_s/h_f = 0.12, 0.04$, Fig. ~~°C as it moves from the shelf to the fjord interior. The cooling of the deep~~

245 ~~fjord water is most significant above ~350 m. Both the structure of the exchange flow and the temperature and density fields over the sill show that a frontal zone is formed near the sill crest (Fig. 3b,~~3c). ~~The front becomes steeper with smaller h_s/h_f as currents accelerate significantly~~ c), a front with increasingly steeper isopycnals and stronger flow develops as the oceanic inflow accelerates over and down the slope after crossing the sill. Strong mixing is observed in this region and results in the upper-layer outflow recirculating before passing the sill, cooling the deep fjord as a result.

250 ~~In order to examine the influence of sill depth on the volume and heat transport, we applied a simplified framework of heat and volume budgets for the fjord . A control volume is defined such that it is bounded by the cross-fjord section S0 near the glacier front, and by the cross-section S2 on the oceanward side of the sill (see Fig. 1). There's no heat exchange with the overlying atmosphere. The time-mean heat flux (H) and volume flux (Q) through the cross-section for two layers, and vertically through the layer interface are calculated (Table **??**, Table **??**), positive values represent fluxes in the down-fjord~~

255 ~~direction and negative values indicate fluxes that are transported in the up-fjord direction. The interface between the~~ In these shallow sill cases, the lower-layer inflow cools by 0.2 to 1 °C as it moves from the shelf to the fjord interior. The cooling of deep fjord water is most significant above ~350 m.
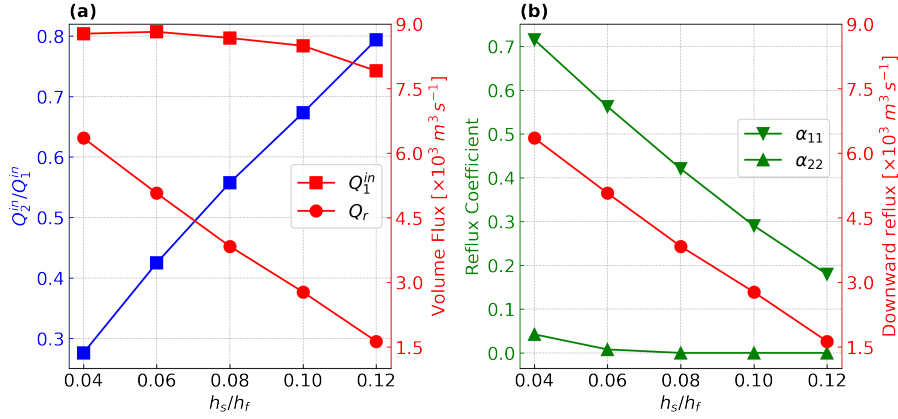
Figure 4. TEF transports (a) and reflux fractions (b) with varying sill depths. 1, 2 denote the cross-fjord section on either side of the sill; Q_1^{in}, Q_2^{in}: volume fluxes of the water flowing into the fjord; Q_r: downward reflux; α_{11} and α_{22} correspond to downward and upward reflux fraction, respectively.

The increased mixing with shallower sills in these two-layer cases is consistent with well-understood fjord dynamics where the flow over the sill can reach a supercritical condition that enhances downstream mixing (Geyer and Ralston, 2011) . Layer-averaged along-fjord velocity and layer salinity are defined as U_{upper}, U_{lower}, and S_{upper}, S_{lower}, respectively. The Froude number, which is greater than 1 when the flow is supercritical, is

$$Fr_{upper} = \frac{U_{upper}}{\sqrt{g'h_{upper}}}, Fr_{lower} = \frac{U_{lower}}{\sqrt{g'h_{lower}}} \tag{5}$$

where $g' = g\frac{\rho_{lower}-\rho_{upper}}{\rho_{lower}}$ is the reduced gravity, ρ, h denote the density and thickness of the upper and lower layers~~was defined kinematically as the zero crossing of the along-fjord velocity profile. As expected, the heat budget of the control volume is dominated by advective processes, with much smaller diffusive heat fluxes (not shown here)~~ . Near the glacier front, both ~~the advective heat flux (H_0^f, H_0^s) and the volume flux (Q_0^f, Q_0^s) slightly decrease with smaller~~ . In the base case simulations, the upper-layer outflow remains subcritical, while the lower-layer Froude number reaches criticality as h_s/h_f ~~in most cases with a shallow sill, indicating the fjord water is cooled~~ falls below 0.06, indicating hydraulic control. The cooling of deep water that results from the enhanced mixing and reflux over the sill can be diagnosed using Eq. (4) (Fig. 5). With a minor ($<4\%$) adjustment to the downward reflux coefficient α_{11}, the theory predicts the deep-water temperature with a coefficient of determination of $r^2 = 0.99$. Both estimated and modeled results show that the deep fjord is 0.1-0.6 °C colder than the shelf water, with shallower sills ~~. In contrast, the heat and volume fluxes close to the fjord mouth (H_2^f, H_2^s and Q_2^f, Q_2^s) are reduced significantly as the sill becomes shallower, adding more constrictions and colder water from the fjord head. Compared to the no-sill case ($h_s/h_f = 1$), the~~ resulting in greater cooling (Fig. 5).
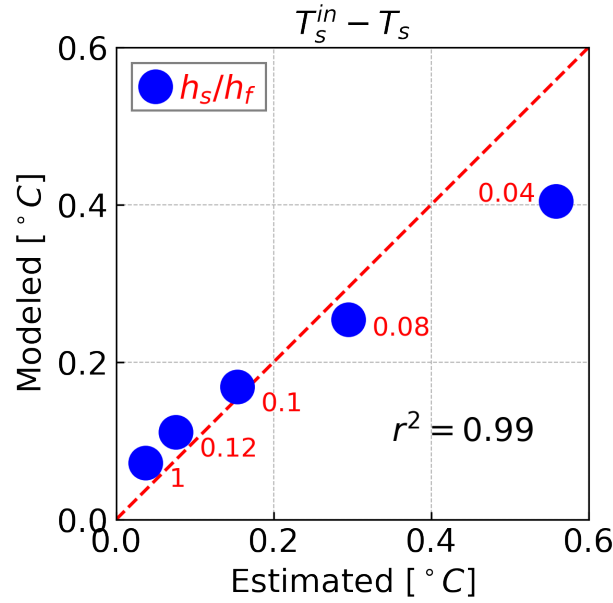
Figure 5. A comparison between the deep water temperature anomaly $(T_s^{in} - T_s)$ estimated from Eq. (4). T_s^{in} is the temperature of incoming oceanic water from the shelf. The reflux coefficient α_{11} is scaled up by 3.5%, results are averaged over the last 14 days of simulations.

275   While the volume transport from the ocean outside the fjord (Q_2^{in}) is drastically reduced when the sill is shallower, this reduction is largely compensated by the increase of reflux into the incoming layer (Q_r). The near-mouth exchange ~~heat and volume~~ fluxes in the shallowest-sill case $(h_s/h_f = 0.04$ ~~) is about~~, Fig. 4a) are approximately 64% smaller ~~.~~

~~Time-mean advective heat flux (H) through the cross-fjord sections and in the vertical. Superscripts f, s, r represent fresher layer, saltier layer, and vertical direction respectively. Subscripts 0, 1, 2 denote the cross-fjord sections S0, S1, and S2.~~ than

280 the no-sill case. As h_s/h_f ~~H_0^f ($\times 10^{11} Js^{-1}$) H_0^s ($\times 10^{11} Js^{-1}$) H_1^f ($\times 10^{11} Js^{-1}$) $H1^s$ ($\times 10^{11} Js^{-1}$) H_2^f ($\times 10^{11} Js^{-1}$) H_2^s ($\times 10^{11} Js^{-1}$) H_r ($\times 10^{11} Js^{-1}$) 0.04 2.51 -2.54 2.83 -2.85 0.87 0.35-0.88 -2.05 510.06 2.78 -2.81 3.09 -3.12 1.32 0.53-1.35 -1.94 490.08 2.96 -2.99 3.2 -3.24 1.69 0.68-1.72 -1.60 400.10 3.05 -3.08 3.19 -3.22 2.00 0.80-2.03 -1.36 34~~decreases from 0.12 ~~2.88 -2.91 2.95 -2.99 2.22 0.89-2.26 -0.73 181 2.38 -2.41 2.45 -2.48 2.49 -2.53~~ to 0.04

~~Time-mean volume flux (Q) through the cross-fjord sections and in the vertical. $f, s, r, 0, 1, 2$ are same as in Table ??. Q_{sm} is submarine melting flux. h_s/h Q_0^f ($m^3 s^{-1}$) Q_0^s ($m^3 s^{-1}$) Q_1^f ($m^3 s^{-1}$) Q_1^s ($m^3 s^{-1}$) Q_2^f ($m^3 s^{-1}$) Q_2^s ($m^3 s^{-1}$)~~, the

285 downward volume transport ~~Q_r ($m^3 s^{-1}$) Q_{sm} ($m^3 s^{-1}$)0.04 7154 -6904 8041 -7792 2447 0.37-2199 -5647 579.920.06 7683 -7433 8514 -8264 3636 0.55-3386 -5188 5210.320.08 8026 -7776 8653 -8404 4571 0.69-4323 -4215 4310.360.10 8159 -7909 8507 -8257 5344 0.81-5094 -3535 3610.520.12 7658 -7408 7849 -7600 5911 0.90-5662 -1899 1910.861 6298 -6048 6466 -6216 6573 -6323 99 9.3~~

290 ~~The impact of~~ increases by a factor of ~ 3. Across the shallow sill cases, the deep incoming transports in the fjord near the sill $(Q_1^{in}$, Fig 4a) and near the ~~sill in the vertical heat and mass exchange at the sill are shown in Table ?? and ??. As~~
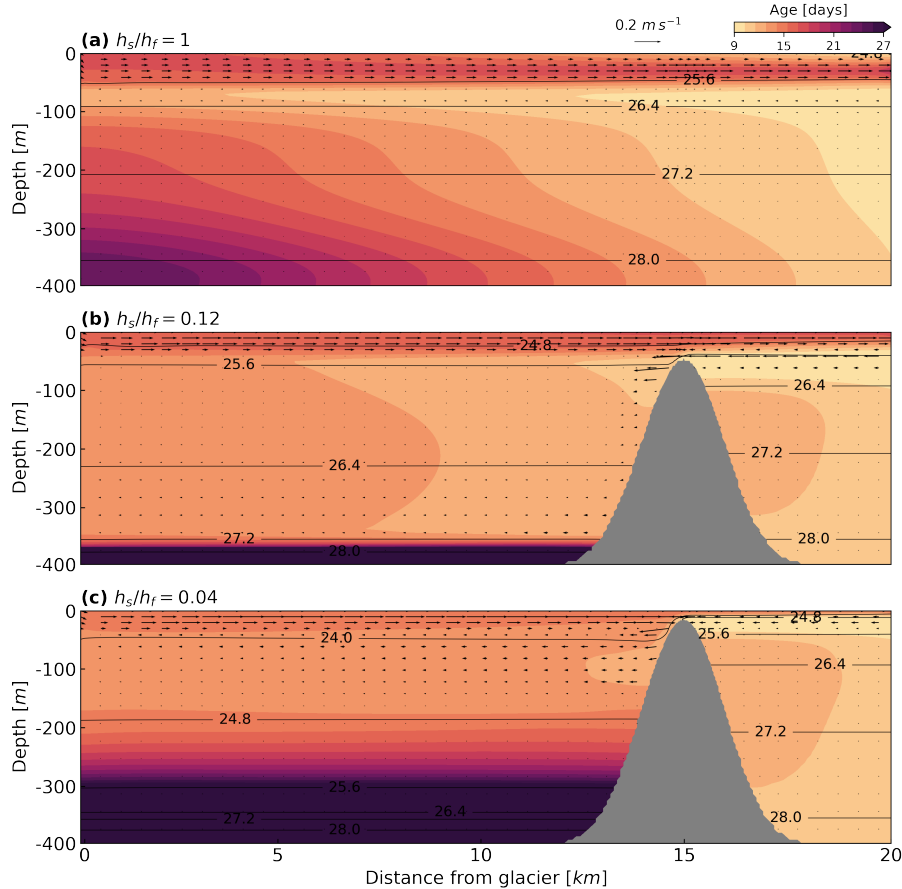
Figure 6. Along-fjord distribution of the shelf water tracer age at the end time (day 60) of simulation. $Q_{sg} = 250\,m^3\,s^{-1}$, black contours denote water density anomaly.

~~expected, the volume and heat fluxes (H_r, Q_r, positive upwards) through the interface separating the upper and lower layers is near zero in the absence of a sill~~glacier (not shown) remain largely unchanged as a result of the increased sill-driven reflux. That is, while a shallow sill does result in strong cooling and reduction of the inflow of oceanic water, it does not significantly change the strength of the circulation within the fjord itself. As the sill becomes shallower, ~~they become increasingly negative, i.e., shallower sills result in enhanced downward transport and cooling of the lower, warm water inflow~~the downward fraction α_{11} increases nearly linearly and is consistent with the variation of reflux Q_r. As h_s/h_f decreases from 0.12 to 0.04, ~~the downward volume transport Q_r and the deeper layer heat loss H_r increases by a factor of ~3, with magnitudes comparable to the horizontal fluxes across the sill. In addition, fluxes at the glacierward side of the sill (H_1^f, H_1^s and Q_1^f, Q_1^s) are comparable with those near the glacier front, indicating that the vertical transport occurs mostly in between sections S1 and S2, and over the sill.~~increases by about $5000\,m^3\,s^{-1}$, and at least 50% more of the outflowing water is refluxed into the deep layer. The upward reflux coefficient α_{22} is close to zero in all these cases (Fig. 4b).

The presence of the sill also impacts the response timescale of the fjord to shelf variability (Fig. 6). The tracer age increases, as expected, with depth and distance from the shelf, and the shelf water takes less than 23 days to reach the entire fjord when there is no sill (Fig. 6a). As the sill becomes shallower and mixing near the sill increases, the maximum intrusion depth in the fjord decreases as more of the lighter outflow is entrained into the inflowing oceanic water. When comparing the velocity and density profiles in Fig. 6b and 6c, the intrusion depth of shelf water decreases from about $350\,m$ to $250\,m$ as the sill ratio h_s/h_f is reduced from 0.12 to 0.04. Consistent with circulation patterns, the tracer age is much lower within the incoming flow than within the near-bottom layer.

The active mixing occurring at the sill can be examined using the Froude number around the sill. Layer-averaged along-fjord velocity and layer salinity are defined as U_{upper}, U_{lower} and S_{upper}, S_{lower} respectively. The Froude numbers are then determined as

$$Fr_{upper} = \frac{U_{upper}}{\sqrt{g'h_{upper}}}, Fr_{lower} = \frac{U_{lower}}{\sqrt{g'h_{lower}}}$$

where $g' = g\frac{\rho_{lower}-\rho_{upper}}{\rho_{lower}}$ is the reduced gravity, ρ, h denote the upper- and lower-layer density and thickness.

Along the channel, the upper-layer outflow remains subcritical while the lower-layer Froude number changes dramatically over the sill as the inflow approaches to being supercritical with shallower sills (not shown). Specifically, as h_s/h_f goes below 0.06, the lower-layer Froude number Fr_{lower} exceeds one at the top of the sill, and an hydraulic jump is formed. With shallower and thus steeper sills, the lower-layer inflow experiences a greater acceleration down the sill, creating a strong velocity shear at the interface with the upper outflow. The enhanced shear and hydraulic transition over the sill lead to conditions favorable for mixing and entrainment of the exchange flow, which are reflected in the enhanced downward flux of heat and mass shown earlier.

TEF transports (a) and reflux fractions (b) with varing sill depths. 1, 2 denote the cross-fjord section on either side of the sill; Q_{in}: volume flux of the water flowing into the fjord; Q_r: downward reflux; α_{11} and α_{22} correspond to downward and upward reflux fraction respectively.

In order to quantify the entrainment to the sill overflow and to estimate the heat supply from the fjord to the glacier, we first calculated the TEF transports at cross-sections (S1 and S2) on both sides of the sill. The temporal average of the TEF inflow and outflow volume flux was defined as Q_{in} and Q_{out}. Based on volume conservation at steady state, the entrainment flux (downward reflux) Q_r across the upper-bounding isohaline surface equals the divergence of inflow or outflow through the segment bonded by two cross-sections (Wang et al., 2017). In the sill segment we defined, the volume fluxes of the exchange flow and the entrainment under different sill depths are characterized using the TEF calculation (Fig. 4).

Changes in volume flow towards the fjord head from section S1 to S2 reveal the modulation of water transport by the sill. With shallower sills, Q_{out}^1 remains almost unchanged while Q_{in}^2/Q_{out}^1 decreases by ~0.5, showing that the water incoming transport (Q_{in}^2) is constrained by the sill. It also suggests other sources of water supply in the sill segment. Noticeably, the reflux over sill (Q_r) increases with smaller h_s/h_f and can reach about 70% of the inflow within the fjord (Q_{out}^1). This process

~~of reflux of the cold upper layerwater into the warmer, lower layer largely compensates for the reduction of the exchange flow at the sill. That is, the exchange circulation in the fjord away from the sill does not weaken significantly, but rather the lower layer becomes colder.~~

340 ~~Consistently with the above, the upward reflux coefficient α_{22} is close to zero in all these cases. As the sill becomes shallower, the downward fraction α_{11} increases nearly linearly and is consistent with the variation of reflux Q_r. As h_s/h_f decreases from 0.12 to 0.04, Q_r increases by about 5000 $m^3 s^{-1}$, and at least 50% more of the outflowing water is refluxed into the deep layer.~~

~~The estimated deep water cooling that results from the reflux process can be reasonably predicted using Eq. (4) (Fig. 5),~~
345 ~~where temperature is non-dimensionalized by T_s^{in}, and their ratio T_{fjord}/T_{shelf}, indicates the relative water temperature in the fjord compared to the shelf-water temperature. With a minor ($< 4\%$) adjustment to the downward reflux coefficient α_{11}, the theory predicts the deep water temperature with a coefficient of determination of $r^2 = 0.99$. Despite some discrepancies, both estimated and modeled results show that the deep fjord is 0.1~1 $^\circ C$ colder than the shelf water depending on the sill depth. In the shallowest sill case ($h_s/h_f = 0.04$), the warm inflow from the shelf is cooled around 10% by the sill-driven~~
350 ~~reflux. A comparison between the deep water temperature estimated from Eq. (4) and from the model. Fjord temperature is non-dimensionalized by shelf-water temperature. Increasing marker sizes correspond to increasing values of sill-fjord depth ratio h_s/h_f.~~

3.2 ~~**Circulation and Heat Transport Regimes**~~

~~The~~

355 **3.2** **Circulation and Cooling Regimes**

The base run discussed in Section 3.1 illustrates the case where the resulting fjord circulation closely resembles a typical shallow-silled ~~fjord-i.e., with no~~ fjord (i.e., without a marine-terminating ~~glacier-where a two layer~~ glacier), where a two-layer exchange flow is formed and strong control on the exchange is exerted by the sill. ~~A key difference , however,~~ However, a key difference is that adding a deep source of buoyancy at the head of the fjord ~~does result in significant~~ results in significant
360 subsurface mixing and cooling of the lower layer. A buoyant plume formed by injection of freshwater at depth and rising through a stratified fluid can result in the plume reaching neutral buoyancy well below the surface. ~~Because this reduces the height from~~ Strong stratification can constrain the plume terminal height and thus reduce the distance from the plume detachment location at the ~~bottom at which the plume detaches from the glacier,~~ glacier, and it also impacts the overall entrainment of warm ambient water~~and resulting submarine meltingdriven by the ascending plume~~, reducing submarine melting.
365 In this section, we focus on how these subsurface plumes interact with a shallow sill, and how the changes in stratification compete with the cooling to modulate the modeled submarine melting rates.

A scaling for the height h_p that a plume generated by a point source of subglacial discharge reaches can be estimated from (Slater et al., 2016):

$$h_p = h_0(N_0^2)^{-3/8}\left(\frac{g_0' Q_{sg}}{2\pi\gamma^2}\right)^{1/4} \tag{6}$$

Based on buoyant plume theory (Morton et al., 1956). The terminal depth depends on the reduced gravity of the plume g_0' as it was evaluated at the grounding line with the fresh plume density and a reference density. It also depends on the entrainment coefficient γ, here taken to be 0.1, and the ambient stratification N_0^2. h_0 is a nondimensional height related to the radius, velocity, and reduced gravity of the plume. We estimated h_0 from five runs with $Q_{sg}=$250 $m^3\,s^{-1}$, using a fixed temperature (10 °C) and an initial salinity increasing linearly in the vertical with a range that represents weakly to strongly stratified glacial fjords.

Fitting the results to Eq. (6) resulted in an empirical coefficient of $h_0 = 1.69$ across this range of initial stratification conditions.

The relative depth of the fjord h_f, the sill h_s, and the initial height of the plume h_p (Eq. (6)) help define four circulation regimes that were evident in our model runs. These are shown schematically in Fig. 7 and further illustrated by model snapshots in Fig. 8. When the initial stratification is relatively weak or the subglacial discharge is relatively strong so that the plume reaches fjord surface and $h_p/h_f = 1$, the circulation is characterized by the near-steady, two-layer exchange flow that we described in the base case, where hydraulic control and the reflux of the cold outgoing plume water into the lower layer are the dominant processes controlling the cooling of the lower layer temperature (Regime I, Fig. 7a, Fig. 8a). When $h_p/h_f < 1$ (i.e., a subsurface plume) and $h_p/(h_f - h_s) > 1$ (i.e., the plume depth is above the sill) a three-layer circulation regime is formed, with a subsurface freshwater overlying oceanic inflow into the fjord (Regime II, Fig. 7b and Fig. 8b). In our runs, the surface layer above the outgoing plume showed a rather weak circulation, and Regime II was transient as the outgoing plume continued to mix and eventually reached the surface, i.e., transitioning to Regime I. However, this relatively fast transition might not generally be the case in fjords with deeper sills, relatively weak subglacial discharge, or relatively strong near-surface stratification. We note that as water properties and stratification evolve over time, the fjord circulation regime might shift, transitioning, for example, from Regime III to Regime I as the plume is initially trapped in the fjord before eventually rising to the surface.

The circulation regimes that lead to the strongest deep cooling are III and IV, that is, when $h_p/(h_f - h_s) \le 1$. In these cases, the freshwater plume cannot exit the fjord, at least initially. The first circulation regime

(Fig. 7c,d, Fig. 8c,d). Regime III shows the outgoing plume reaching the sill and forming ~~an~~ a horizontal recirculation. Heat ~~being~~ drawn from the deep fjord waters by submarine melting at the ice face and entrainment of warm ocean water into the outgoing plume cannot be replaced with exchange with the shelf, and thus the deep fjord continues to cool ~~as~~ because the heat budget, in this case, is fundamentally unsteady. The subsurface (and sub-sill) plume continues to mix with the surrounding waters, rising in the process (Fig. 8c). ~~While not allof~~ Some, but not all, of our Regime III cases eventually reached the sill depth during ~~our $h_p/(h_f - h_s) < 1$ cases reached this state in our~~ 60-day runs, ~~some did show the plume eventually reaching the sill depth,~~ allowing the plume to exit the fjord and thus forming a last distinct circulation~~regime,~~ Regime IV. In this configuration, the circulation resembles a reverse estuary, where the exchange is either lateral or vertical (Fig. 8d), but outflow is concentrated just above the sill. However, this regime is also fundamentally unsteady because heat entrained into the outgoing plume from the deep water in the fjord cannot be readily replaced with exchange with the shelf, leading to continuous cooling of that layer as well.

In Regime III cases, the plume remains trapped below the sill for periods ranging from a few days to the entire 60-day run, suggesting that this process might be relevant for understanding seasonal-scale changes in fjord circulation and melting regimes. We can approximate this problem by assuming that the fjord below the sill acts as a 'filling box' (Baines and Turner, 1969), where the outflowing plume progressively fills the basin downward from the initial level of neutral buoyancy. Cardoso and Woods (1993) provided an estimate of the timescale t_a for a horizontal plume in a linearly stratified environment to ascend (or 'fill the box') as

$$t_a = 0.12\gamma^{-4/3}H_0^{-2/3}AB^{-1/3}\tau \tag{7}$$

where $H_0 = h_p/(2^{5/8}h_0)$ is a characteristic length scale (Morton et al., 1956) proportional to the initial plume height h_p in Eq. (6), A is the horizontal cross-section area from the glacier front to the sill, $B = g_0' Q_{sg}$ is the buoyancy flux of the plume. This approximation assumes that the contribution to B from submarine melting is negligible. The nondimensional time τ can be obtained from

$$\tau = 2^{-7/3}\left(\left(\frac{h_f - h_s}{H_0}\right)^2 - 2.4^2\right) \tag{8}$$

As the initial plume height h_p decreases with the prescribed initial stratification increasing from $1N_0^2$ to $4N_0^2$, the plume takes longer to reach the crest of the sill (Fig. 9a-d). Eq. (7) gives a reasonable estimate of the timescale for the plume rising to the sill level and leaving the fjord (Fig. 9e), ranging from less than 10 days to about 6 weeks. While the initial stratification leading to these estimates is prescribed, this suggests that Regime III cases can last for a significant period.

In summary, we find that for cases where the circulation regime is dominated by a ~~two or three layer exchange flow at the sill~~ two- or three-layer exchange flow above the sill depth (Regimes I and II), with inflow from the ocean at depth, the dynamics of sill-driven mixing and reflux discussed in the base case are critical to understanding how deep fjord properties will evolve. In

these cases, a steady view of the circulation in at least seasonal ~~time scales~~ timescales is reasonable, as deep heat supply from the shelf balances the heat ~~exchange at the mouth of the fjord can compensate for the heat~~ loss due to mixing and melting ~~.~~ (Fig. S3, S4). But when either strong stratification or weak subglacial discharge leads to a deep (relative to the sill) outflowing plume, as in Regime III, cooling of the deep fjord is not caused by ~~reflux but rather mixingof warm water into the plume which~~ sill-driven advection and mixing, but the continuous removal of heat from the deep layer of the fjord that cannot be replaced by ~~exchange with the shelf~~an oceanic inflow. Critically, this means that the properties in the fjord ~~are strongly time dependent~~can be strongly time-dependent in synoptic to seasonal timescales, and sill processes become less important until the plume reaches the sill crest.

~~The along-fjord velocity (a), temperature (b) profiles corresponding to Regime I-IV, and the impact of shallow sill vs. fjord stratification on near-glacier temperature and submarine melting. Vertical profiles in (a) and (b) are collected at section S1, results in (c) are averaged over the last 14 days of the simulation.~~

3.3 The Competing Impacts of Deep Stratification and Temperature Changes on Submarine Melting

~~The evolution of submarine melting (a, b), near-glacier temperature (c, d), and near-glacier stratification (e, f) with (left panel) and without (right panel) a sill. Both cases have the same initial stratification ($1N_0^2$) and mostly fit in Regime I.~~

~~The regimes are defined from the interaction between stratification and the sill , thereby the variations in fjord stratification and sill depth may have major impacts on the circulation structure, heat transport pattern, and therefore melting at the glacier front. Figure 10a, b show the vertical profiles of along-fjord velocity and temperature inside the fjord corresponding to the four distinct regimes, which are identified at different time with varied stratification and sill depth. As water properties and stratification change over time, the fjord circulation may fit into diverse regimes from the beginning to the end of simulations. Consistent with the effect of sill-driven reflux and heat transport regimes, water column temperature~~ While the sill restricts the inflow of warm oceanic water to the fjord and reflux from the freshwater plume results in cooling of the deep water near the glacier~~front indicate a fjord cooling caused by a shallow sill and stronger initial stratification (Fig. 10c) . In addition, the relative impact between stratification and the shallow sill on submarine melting showed that the reflux driven by a shallow sill increasedthe melting compared to all the~~, submarine melting is often larger in runs with shallow sills compared to equivalent no-sill runs. Submarine melting (Q_{sm}) was slightly higher with shallow sills in our base case (Fig. 3) and consistently so in the cases discussed in Section 3.2, where Q_{sm} decreased for all cases as the linear stratification increased, but it was also lower for the no-sill cases (~~Fig~~$h_s/h_f = 1$, Fig. 10). ~~10c). To understand this counter-intuitive effect from sill-driven reflux, the variation of submarine melting,~~

The perhaps counterintuitive result of submarine melting increasing as deep cooling is enhanced by shallow sills can be understood by considering that sill processes also decrease stratification, which has the opposite effect on submarine melting. This competition is illustrated in Fig. 11, which shows the evolution of near-glacier temperature and stratification ~~are presented in Fig. 11. Except at the very beginning of simulation with the shallowest sill , both cases coincide with~~for two cases with the same initial and forcing conditions other than the presence of a shallow sill. But for a brief period at the start of the shallow sill run (Fig. 11a,b), both cases are examples of Regime I, where ~~the plume drives~~a surface outflow is generated. When there is no

sill ($h_s/h_f = 1$), the melting (Fig. S5), fjord temperature, and stratification ~~remained stable throughout the entire~~ remain nearly constant throughout the simulation (Fig. 11b, d~~, f~~). With ~~the presence of~~ a shallow sill ($h_s/h_f = 0.04$), however, ~~submarine melting became higher especially after around~~ cooling is overwhelmed by the collapse of stratification in the deep water to increase submarine melting, particularly after 30 days or so (Fig.~~11a~~ S5). During that period, the fjord temperature dropped ~~continuously~~ as expected from the cooling effect of sill-driven reflux (Fig.~~11e~~ 11a). Meanwhile, the fjord stratification became significantly weaker due to ~~the~~ strong mixing with the refluxed plume outflow and the sill impeding the inflow of denser shelf waters into the fjord (Fig.~~11e). The fjord cooling and the decreased stratification both induced by sill-driven reflux have opposite impacts on glacial melt, and in our cases here the effect from stratification is more pronounced than that from fjord temperature, resulting in less heat supply to the glacier but increased submarine melting.~~ 11c).

~~In general, the sill-driven reflux and the heat supply towards glaciers are impacted in different circulation regimes. With a surface or subsurface outflow in Regime I and II~~

The competition between the decrease of stratification and cooling driven by the presence of the sill is further illustrated in Fig. 12, which shows Q_{sm} as a function of initial stratification and fjord temperature. Q_{sm} is proportional to $T_{af}(N^2)^{-5/8}$, where $T_{af} = T_a - T_0$ is the divergence between the modeled ambient temperature T_a and the freezing temperature of seawater T_0 (Slater et al., 2016). We used a linear fit (Fig.~~7a, b), the plume water being refluxed is modulated by the sill depth and subglacial discharge, and it cools the deep fjord by drawing down significant amount of cold water. When the discharge is weak or~~ S6) to find the constant of proportionality between the modeled Q_{sm} and the scaling above. Several runs with constant initial and forcing conditions, but where a shallow sill is added, are shown here, the markers are color-coded with the magnitude of the modeled Q_{sm}.

Consistent with Fig. 11, the ~~ambient stratification is strong,~~ results indicate that the lowering of deep water stratification caused by the presence of the ~~plume enters the fjord at a height below the sill, in which case the reflux is barely generated while the plume-driven outflow fills and cools the fjord basin progressively (Fig. 7c). As mixing continues and the plume rises to a higher level right above the sill, the circulation pattern in Regime IV (Fig. 7d) can also be viewed as a transition period from Regime III to Regime II and I. Based on our simulations, the unsteady scenario of Regime IV may last at least for a seasonal timescale, the deep fjord is continuously cooled by the mixing with outgoing plume and the sill-driven reflux~~ sill has an equal or greater impact on submarine melting than the cooling that occurs there. We note that we ran no-sill cases only for a subset of our sill runs. Fjords where adjacent deep waters are warm with relatively low stratification (e.g., Jorge Montt in Patagonia) might be an example of this outcome, while Greenland fjords where the ambient waters are relatively cold might be less so. From considering the relative changes to $T_{af}(N^2)^{-5/8}$ with respect to N^2 and T_{af}, we would expect that the change in deep temperature ΔT_{af} (i.e., the change in deep temperature across the sill caused by the presence of the sill) must exceed $\frac{5T_{af}}{8N^2}\Delta N^2$ to generate a net increase in submarine melting. And ΔN^2 is the equivalent and competing change in stratification across the sill.

Our results indicate that the impact of shallow sills on submarine melting in glacial fjords depends on the competition between cooling and the decrease of stratification caused by the presence of the sill. The only source of these changes in

Table 2. Tidal-exchange velocity ratio (U_t/U_e), ~~outflow volume transport at S1~~ downward reflux over the sill (Q_1^{out} Q_r), downward reflux fraction (α_{11}), ~~downward~~ upward reflux ~~over sill~~ fraction (Q_r α_{22}), ~~fjord-shelf temperature ratio (T_{fjord}/T_{shelf}),~~ submarine melting (Q_{sm}), mean temperature (T) and stratification (N^2) near the glacier front for tidal experiments with $Q_{sg} = 250\ m^3\ s^{-1}$ and $h_s/h_f = 0.04$.

U_t/U_e	Q_1^{out} Q_r ($m^3 s^{-1}$)	α_{11} (%)	Q_r ($m^3 s^{-1}$) T_{fjord}/T_{shelf} α_{22} (%)	Q_{sm} ($m^3 s^{-1}$)	T_s (°C)
0	~~9025~~ 6352	71.5	~~6352~~ 4.2	~~95.9~~ 10.5	~~9.9~~ 9.2
0.7	~~9006~~ 6330	70.3	~~6330~~ 4.4	~~95.9~~ 10.5	~~7~~ 9.2
1.3	~~9018~~ 5562	~~67.7~~ 63.8	~~6104~~ 8.2	~~95.9~~ 10.5	~~7 1.6~~ 9.2
~~1.9 10389 46.7 4852 95.8 10.6 6.94~~ 6.5	~~24877~~ 8047	~~21.0~~ 53.0	~~5229~~ 15.2	~~95.8~~ 12.9	~~5.55~~ 9.7

deep-water properties is the interaction between the sill and plume-driven circulation. The impact of tidal currents, which can
500 be an important source of mixing in fjords, is briefly explored next.

3.4 The Impact of Tides

Tides are another important process that modulates the ~~inflow of warm shelf waters in fjords and promotes turbulence and mixing . In a non-dimensional format, we use the ratio of the maximum tidal current amplitude~~ circulation and mixing rates in fjords. We ran ten additional simulations with a shallow sill configuration ($h_s/h_f = 0.04, 0.12$) and varying tidal amplitudes at
505 the eastern boundary of the model (see Methodology) to force a range of tidal velocities at the sill (U_t) relative to the exchange flow ~~velocity~~ U_e ~~at the sill to illustrate the strength of tidal forcing.~~ U_t is ~~obtained~~ estimated at the sill ~~using tidal harmonic analysis~~ from harmonic analysis (Codiga, 2011). U_e is ~~scaled by~~ estimated from

$$U_e = \frac{Q_e}{A_{sill}/2} \tag{9}$$

where Q_e is the exchange flow transport defined as $(Q_{out} + Q_{in})/2$ ~~(,~~ Q_{in}, Q_{out} are positive ~~)~~ and A_{sill} is the cross-channel
510 area at the sill crest. In the tidal simulations, U_t ranges ~~between~~ from 0.1 to 1 $m\,s^{-1}$ and U_e ~~has little variation, ranging between~~ is nearly constant, ranging from 0.13 to 0.15 $m\,s^{-1}$. ~~With the shallowest sill ($h_s/h_f = 0.04$), the exchange in the fjord,~~ The sill-driven reflux Q_r, deep fjord temperature T_s, and submarine melting ~~before and after the tidal forcing is applied~~ with and without tidal forcing are summarized in Table ~~2.~~ 2. The results are averaged over the last 14 days of simulations.

~~With higher tidal velocity, the along-fjord exchange (Q_e) is enhanced by the flood and ebb tides as expected. In contrast,~~
515 Increasing tidal forcing leads to a reduction in the downward reflux fraction and an increase in the upward reflux fraction, with varying impacts on the downward reflux ~~fraction (α_{11}) decreased significantly~~ Q_r. The outflow increases with stronger tidal forcing due to enhanced exchange flow along the fjord, particularly as the tidal velocity ~~surpassing~~ exceeds the exchange velocity ($U_t/U_e > 1$). ~~In most cases, the reflux volume at the sill (Q_r) also decreased with stronger tides , as a result of increased exchange flow but more reduced reflux fractions. As for the deep-fjord temperature, it remained more or less the same since the~~
520 ~~magnitude of water exchange did not change much across all these runs. Still, submarine melting Q_{sm} increased by 6% to 30%~~

The increase in the upward reflux fraction (α_{22}) with tides reflects enhanced vertical exchange. A small (5%) increase in melting is evident for the weakest tidal forcing case relative to the no-forcing case. For tidal cases with U_t/U_e between 0.7 and 1.3, the small changes in reflux magnitude did not have a meaningful impact on the stratification, deep-water temperature, or submarine melting. The strongest tidal forcing case we ran did result in weakening of stratification and a warmer fjord compared to the other cases (Fig. S7), which is reflected in the highest melting rate. The warm outflow in this case is also enhanced by the upward entrainment flux and gets largely (> 50%) refluxed into the deep fjord. Overall, the decrease in the reflux fraction is consistent with the results from Hager et al. (2022), but fully understanding the impact of tidal forcing in these systems requires further study.

4 Discussion

4.1 Application to Realistic Fjord Systems

The sill reflux process described above has been discussed in observational studies in both non-glacial and glacial fjords. In Loch Sunart, a shallow-silled Scottish fjord, hydrographic and current meter data collected during the summers of 1987, 1989, and 1990 revealed that an estimated 20% to 70% of the surface water recirculated into the bottom layer (Gillibrand et al., 1995). At Godthåbsfjord, Greenland, the summer surface water in the sill region was observed to reach the glacier terminus at depth, with the subsurface freshwater fraction increasing from winter (3%) to summer (10%) (Mortensen et al., 2013). The authors highlighted a mixing process at the sill that resembles the reflux of glacial freshwater that we focus on here. Most recently, observations in LeConte Bay, Alaska ($h_s/h_f = 0.06$) showed that 50% to 75% of the summer inflow was composed of refluxed plume-driven outflow (Hager et al., 2022). This range is comparable to our base case simulations (Fig. 4b).

The circulation regimes identified here (Fig. 7) suggest that conceptual models of glacier melting where the circulation and heat budget of the fjord are steady might not always be adequate. When a buoyant plume flowing away from the glacier is blocked by the sill (Regime III) or barely reaches the sill level (Regime IV), the system is temporarily unsteady as the plume continues to rise and the deep water below is cooled. During the summer, glacial fjords in Greenland (Mortensen et al., 2013), Alaska (Hager et al., 2022), and Patagonia (Moffat et al., 2018) show intense subglacial discharge and surface or subsurface plume outflow as in Regimes I and II (Fig. 7a, b). With stronger ambient stratification or weaker winter subglacial discharge, buoyant plumes enter the fjord at depth, forming an outflow that intersects the sill or is mostly blocked by it (Gladish et al., 2015; Carroll et al., 2016), resembling Regime

III (Fig. 7c), in which case the blocked outflowing plume is expected to progressively cool the deep fjord. ~~We were not able~~ In the fall-winter circulation regime at LeConte Bay, Alaska (Hager et al., 2022), the reduced freshwater outflow could be blocked by a shallow sill, recirculated as in Regime III. In that system, however, strong tidal currents also play an important role in exchange across the sill. We were unable to find published reports ~~of~~ on Regime IV (Fig. 7d), ~~a kind of reverse estuary circulation (e.g., Giddings and MacCready, 2017),~~ perhaps because this circulation could quickly transition to Regime II or I. Because ~~Regime~~ Regimes III and IV reflect an unsteady state for the ~~heat budget for~~ temperature and stratification of the fjord, ~~and~~ both of which impact the melting rate ~~depends on the resulting deep fjord temperature~~, caution should be used when applying a melting parameterization that assumes a steady ~~circulation in the ocean~~ fjord circulation.

Our simplified model configuration ~~necessarily removes what possibly be key processes modulating~~ ignores what are possibly key processes that modulate both the reflux process and its impact on the heat supply to the ice. While we ~~explored tidal variability briefly~~ briefly explored the tidal variability, the reason for the reduction of the reflux fraction under stronger tidal currents, also reported by Hager et al. (2022), is not well understood ~~, and will be explored in a future study~~. Wind forcing is a ~~well known factor influencing exchange between proglacial~~ well-known factor influencing the exchange between glacial fjords and the open ocean (Straneo et al., 2010; Jackson et al., 2014; Moffat, 2014). Finally, we did not fully explore how more realistic ~~sill depths~~ shelf properties, multiple sills, or different fjord widths ~~might influenced the processes~~ could influence the processes investigated here. However, we believe that the regimes discussed above still provide a useful framework to move forward.

4.2 Implications for Glacial Melt

Our results show that the downward transport of outflowing glacial freshwater at the sill cools the fjord, which is ~~not entirely surprising~~ consistent with previous studies. Although the sill-fjord depth ratio h_s/h_f has a significant impact on the downward reflux fraction (Fig. 4b), the magnitude of reflux and thus the warm water supply ~~towards~~ to glaciers are largely determined by the strength of subglacial discharge, especially with a shallower sill. Depending on the properties of the outflow, the sill-driven reflux may have ~~either reduce or increase~~ reduced or increased heat transport to the glacier. For example, numerical experiments by Hager et al. (2022) found that the warmest surface water during the summer was refluxed and transported to ~~LeConte Glacier terminus~~ the terminus of the LeConte Glacier, enhancing heat supply and submarine melting. ~~In contrast, our results show the heat flux towards the glacier near the glacier front (H_f^0) only has slight variation with different sill depths (Table ??), because the reflux of cold outflow cools shelf water as they cross the sill, but the circulation remains intense in the fjord.~~

~~In our simulations,~~ One key result from our study is that the presence of ~~the sill generates several circulation regimes, two of which have been observed in several systems (I and II), and another for which some evidence exists (IV). In the former, the reflux process~~ a sill leads to a decrease in both temperature and stratification of the deep inflow, ~~which has competing~~ with opposing effects on the rate of submarine melting. In our simulations, the stratification effect ~~generally overcame the cooling~~ is generally greater than the cooling effect, leading to higher submarine melting for ~~the~~ shallow sill cases. However, several caveats should be ~~considered: first, depending on the shelf water structure outside the fjord, a~~ noted: First, our results depend

on the erosion of fjord stratification that is prescribed as an initial condition–the same as for the outside shelf, for convenience, rather than the result of a more realistic evolution. The underlying assumption is that the fjord stratification is changing, for

590 example, from winter to summer, and is set before the onset of a large change in the subglacial discharge, but that evolution is not modeled explicitly. Second, the temperature structure we use is rather simple to keep the parameter space reasonable, but it is common to observe multiple distinct deep water masses outside glacial fjords. For example, a shallow sill might favor overall warmer waters entering the fjord, as it happens in Jorge Montt ~~glacier. More critically, glacial melt away from discrete subglacial discharge outlets freshens the adjacent fjord water and drives weak buoyant plumes (Magorrian and Wells, 2016).~~

595 ~~This ambient melting considered to be negligible in our model, but has been shown to~~ fjord, where a subsurface temperature maximum is found at about sill level outside the fjord (Moffat et al., 2018). Despite this complexity, our results highlight the importance of understanding the processes controlling not only deep-water temperature but also stratification in these systems.

Ambient melting is likely too small in our study, given that observations show that it can be a significant ~~part~~ fraction of

600 the total submarine meltwater flux ~~in real systems (Jackson et al., 2020). These~~ (Jackson et al., 2020). Modeling shows that these background melt plumes also entrain fjord waters and intrude into the fjord after reaching neutral buoyancy ~~. However, it is unclear whether systems where background melting dominates the freshwater output can be conceptualized using discrete plumes as we did here. Additionally,~~ (Magorrian and Wells, 2016). The coefficients used in submarine melt parameterization are derived from ~~ice shelf studies (Cowton et al., 2015), hence~~ studies on ice shelves (Cowton et al., 2015), so the dy-

605 namics and morphology in the near-ice zone ~~might~~ could be substantially different ~~at~~ in tidewater glaciers (Jackson et al., 2022). ~~Point-source~~ Estimates of near-glacier fjord circulation also show that the point-source representation of plume geometry is likely to underestimate entrainment and ~~plume-drive melt , according to measurements of near-glacier circulation (Jackson et al., 2017). As a result, models like we use here are likely to generate submarine melt rates that are far too low in most cases.~~

610 plume-driven melt (Jackson et al., 2017). Despite these important caveats, the fundamental dynamics that lead to retention of meltwater and resulting unsteady ~~state~~ circulation regimes and property budgets in shallow-silled fjords, the competing effects of cooling and destruction of stratification of the sill on melting rates, and the importance of reflux processes ~~are~~ at the sill are likely to be at play in real systems ~~or~~ even as improved models that include background melting and other ~~important corrections~~ processes are developed.

615 ## 5 Conclusions

Mixing and advection processes on shallow sills separating glacial fjords from the open ocean play a critical role in modulating the circulation and ~~heat supply to~~ deep water properties near marine-terminating glaciers. Using a coupled plume-ocean fjord model, we find four circulation regimes that depend on the ratios of the sill depth h_s, the fjord depth h_f, and the depth of the meltwater plume depth h_p. In the first two regimes, the outgoing meltwater plume flows above the sill, either at the surface

620 (I) or below it (II), resembling a more typical (i.e., non-glacial) ~~,~~ steady fjord exchange, where the heat lost to ice melting

can be replaced by oceanic sources. In the other two regimes, however, the plume is either trapped within the fjord by the sill (III) or exits just above it (IV). In either case, the deep fjord layer continues to lose heat as exchange with the open ocean is ~~blocked~~restricted, and the relatively cold subglacial discharge is continuously being mixed into the deep fjord. In our 60-day simulations, these unsteady state conditions can last for the entire run, suggesting that even in seasonal ~~time scales~~ timescales

625 the assumption that a marine-terminating glacier will respond to changes in shelf conditions might be flawed, at least in some cases. The duration of unsteady Regime III depends on the initial depth of the plume, the depth of the sill, and the magnitude of the subglacial discharge.

In the regimes where a ~~steady state~~ steady-state solution is possible (I and II) and the meltwater plume exits the fjord, strong vertical exchange (reflux) is induced over the sill. The exchange is dominated by the downward transport of cold outflow from

630 the upper layer to the warm inflowing water from the ocean, thus contributing to a significant recirculation within the fjord. With a sill depth of $h_s/h_f = 0.04$, about 70% of the plume-driven outflow is refluxed to depth. ~~A range of simulations show that the fraction of the outflow being refluxed is partially controlled by the sill-fjord maximum depth ratio h_s/h_f, and that increasing the subglacial discharge, and hence the outgoing meltwater outflow from the fjord, increases the reflux as well.~~ Critically, we find that the ~~sill processes in those circulation regimes result in a decrease of both~~ presence of the sill results in the reduction

635 of both the deep fjord temperature and stratification near the glacier terminus, which have opposite effects ~~in the melting rate of the glacier~~on the glacial melt rate. In our simulations, the stratification effect tended to dominate, resulting in higher melting even though the incoming ocean water was cooled at the sill. However, recent observational studies (Jackson et al., 2020, 2022) suggest caution in evaluating the overall magnitude of melting we see in our simulations~~as key processes, including~~, as the background melting away from regions of subglacial melting input ~~not represented~~is not adequately quantified in our model,

640 and might have a much larger role than previously thought. However, the generation of the circulation regimes we discuss here ~~are~~is more strongly tied to the formation of subsurface (meltwater plumes, including below the sill~~depth) meltwater plumes~~, regardless of what fraction of that meltwater is of subglacial origin or melted locally.

Overall, our simulations show that vertical exchange at the sill significantly modulates ~~heat supply to tidewater glaciers terminated~~ the circulation and deep-water properties (temperature and stratification being the most critical) in shallow-silled

645 ~~fjords, through the sill-driven reflux of glacial freshwater~~glacial fjords. The relative depth of the plume outflow, the fjord, and the sill provides a useful framework to characterize the circulation and heat transport patterns in ~~glacial fjords~~these systems.

Data availability. The IcePlume package for MITgcm can be accessed at https://doi.org/10.5281/zenodo.7086069. The model output and code used in the analysis are available from the authors upon request (wbao@udel.edu).

Author contributions. W.B. and C.M. conceived the study. W.B. conducted the modeling and led the writing of the manuscript. C.M. assisted

650 with the interpretation of the results and editing of the text.

Competing interests. The contact author has declared that neither of the authors has any competing interests.

Acknowledgements. W.B. was supported by a fellowship from the School of Marine Sciences and Policy, University of Delaware. C.M. received support from ~~COPAS Coastal~~ the COPAS Coastal program (ANID FB210021)~~program~~. Both authors were supported by the University of Delaware Research Foundation Grant #18A00956. We thank Dustin Carroll ~~for his help~~ and Tom Cowton for their assistance in setting up the IcePlume model. This research was ~~supported in part through the use of Information Technologies (IT)~~ conducted using the High-Performance Computing resources at the University of Delaware~~, specifically the high-performance computing resources~~. We thank Rebecca Jackson and a second anonymous reviewer for their thoughtful and constructive comments on the manuscript.

References

Arneborg, L., Erlandsson, C. P., Liljebladh, B., and Stigebrandt, A.: The rate of inflow and mixing during deep-water renewal in a sill fjord, Limnology and Oceanography, 49, 768–777, https://doi.org/10.4319/lo.2004.49.3.0768, 2004.

Baines, W. D. and Turner, J. S.: Turbulent buoyant convection from a source in a confined region, Journal of Fluid Mechanics, 37, 51–80, https://doi.org/10.1017/S0022112069000413, publisher: Cambridge University Press, 1969.

Bartholomaus, T. C., Stearns, L. A., Sutherland, D. A., Shroyer, E. L., Nash, J. D., Walker, R. T., Catania, G., Felikson, D., Carroll, D., and Fried, M. J.: Contrasts in the response of adjacent fjords and glaciers to ice-sheet surface melt in West Greenland, Annals of Glaciology, 57, 25–38, 2016.

Cardoso, S. S. and Woods, A. W.: Mixing by a turbulent plume in a confined stratified region, Journal of Fluid Mechanics, 250, 277–305, publisher: Cambridge University Press, 1993.

Carroll, D., Sutherland, D. A., Hudson, B., Moon, T., Catania, G. A., Shroyer, E. L., Nash, J. D., Bartholomaus, T. C., Felikson, D., Stearns, L. A., Noël, B. P. Y., and van den Broeke, M. R.: The impact of glacier geometry on meltwater plume structure and submarine melt in Greenland fjords, Geophysical Research Letters, 43, 9739–9748, https://doi.org/10.1002/2016GL070170, 2016.

Carroll, D., Sutherland, D. A., Shroyer, E. L., Nash, J. D., Catania, G. A., and Stearns, L. A.: Subglacial discharge-driven renewal of tidewater glacier fjords, Journal of Geophysical Research: Oceans, 122, 6611–6629, 2017.

Codiga, D. L.: Unified tidal analysis and prediction using the UTide Matlab functions, https://doi.org/10.13140/RG.2.1.3761.2008, 2011.

Cokelet, E. D. and Stewart, R. J.: The exchange of water in fjords: The efflux/reflux theory of advective reaches separated by mixing zones, Journal of Geophysical Research: Oceans, 90, 7287–7306, 1985.

Cowton, T., Slater, D., Sole, A., Goldberg, D., and Nienow, P.: Modeling the impact of glacial runoff on fjord circulation and submarine melt rate using a new subgrid-scale parameterization for glacial plumes, Journal of Geophysical Research: Oceans, 120, 796–812, 2015.

Geyer, W. and Ralston, D.: The dynamics of strongly stratified estuaries, in: Treatise on Estuarine and Coastal Science, pp. 37–52, Amsterdam, Elsevier, 2011.

Geyer, W. R. and Cannon, G. A.: Sill processes related to deep water renewal in a fjord, Journal of Geophysical Research: Oceans, 87, 7985–7996, 1982.

Geyer, W. R. and MacCready, P.: The Estuarine Circulation, Annual Review of Fluid Mechanics, 46, 175–197, https://doi.org/10.1146/annurev-fluid-010313-141302, 2014.

Giddings, S. N. and MacCready, P.: Reverse Estuarine Circulation Due to Local and Remote Wind Forcing, Enhanced by the Presence of Along-Coast Estuaries, Journal of Geophysical Research: Oceans, 122, 10 184–10 205, https://doi.org/10.1002/2016JC012479, 2017.

Gillibrand, P. A., Turrell, W. R., and Elliott, A. J.: Deep-Water Renewal in the Upper Basin of Loch Sunart, a Scottish Fjord, Journal of Physical Oceanography, 25, 1488–1503, https://doi.org/10.1175/1520-0485(1995)025<1488:DWRITU>2.0.CO;2, 1995.

Gladish, C. V., Holland, D. M., Rosing-Asvid, A., Behrens, J. W., and Boje, J.: Oceanic Boundary Conditions for Jakobshavn Glacier. Part I: Variability and Renewal of Ilulissat Icefjord Waters, 2001–14, Journal of Physical Oceanography, 45, 3–32, https://doi.org/10.1175/JPO-D-14-0044.1, 2015.

Hager, A. O., Sutherland, D. A., Amundson, J. M., Jackson, R. H., Kienholz, C., Motyka, R. J., and Nash, J. D.: Subglacial Discharge Reflux and Buoyancy Forcing Drive Seasonality in a Silled Glacial Fjord, Journal of Geophysical Research: Oceans, 127, e2021JC018 355, https://doi.org/10.1029/2021JC018355, 2022.

Hager, A. O., Sutherland, D. A., and Slater, D. A.: Local forcing mechanisms challenge parameterizations of ocean thermal forcing for Greenland tidewater glaciers, EGUsphere, pp. 1–33, https://doi.org/10.5194/egusphere-2023-746, publisher: Copernicus GmbH, 2023.

Holland, D. M. and Jenkins, A.: Modeling Thermodynamic Ice–Ocean Interactions at the Base of an Ice Shelf, Journal of Physical Oceanography, 29, 1787–1800, https://doi.org/10.1175/1520-0485(1999)029<1787:MTIOIA>2.0.CO;2, 1999.

Hugonnet, R., McNabb, R., Berthier, E., Menounos, B., Nuth, C., Girod, L., Farinotti, D., Huss, M., Dussaillant, I., Brun, F., and Kääb, A.: Accelerated global glacier mass loss in the early twenty-first century, Nature, 592, 726–731, https://doi.org/10.1038/s41586-021-03436-z, 2021.

Inall, M., Cottier, F., Griffiths, C., and Rippeth, T.: Sill dynamics and energy transformation in a jet fjord, Ocean Dynamics, 54, 307–314, 2004.

Jackson, R. H. and Straneo, F.: Heat, Salt, and Freshwater Budgets for a Glacial Fjord in Greenland, Journal of Physical Oceanography, 46, 2735–2768, https://doi.org/10.1175/JPO-D-15-0134.1, 2016.

Jackson, R. H., Straneo, F., and Sutherland, D. A.: Externally forced fluctuations in ocean temperature at Greenland glaciers in non-summer months, Nature Geoscience, 7, 503–508, https://doi.org/10.1038/ngeo2186, 2014.

Jackson, R. H., Shroyer, E. L., Nash, J. D., Sutherland, D. A., Carroll, D., Fried, M. J., Catania, G. A., Bartholomaus, T. C., and Stearns, L. A.: Near-glacier surveying of a subglacial discharge plume: Implications for plume parameterizations: SUBGLACIAL PLUME STRUCTURE AND TRANSPORT, Geophysical Research Letters, 44, 6886–6894, https://doi.org/10.1002/2017GL073602, 2017.

Jackson, R. H., Nash, J. D., Kienholz, C., Sutherland, D. A., Amundson, J. M., Motyka, R. J., Winters, D., Skyllingstad, E., and Pettit, E. C.: Meltwater Intrusions Reveal Mechanisms for Rapid Submarine Melt at a Tidewater Glacier, Geophysical Research Letters, 47, e2019GL085 335, https://doi.org/10.1029/2019GL085335, 2020.

Jackson, R. H., Motyka, R. J., Amundson, J. M., Abib, N., Sutherland, D. A., Nash, J. D., and Kienholz, C.: The Relationship Between Submarine Melt and Subglacial Discharge From Observations at a Tidewater Glacier, Journal of Geophysical Research: Oceans, 127, e2021JC018 204, https://doi.org/10.1029/2021JC018204, 2022.

Kimura, S., Holland, P. R., Jenkins, A., and Piggott, M.: The Effect of Meltwater Plumes on the Melting of a Vertical Glacier Face, Journal of Physical Oceanography, 44, 3099–3117, https://doi.org/10.1175/JPO-D-13-0219.1, 2014.

Large, W. G., McWilliams, J. C., and Doney, S. C.: Oceanic vertical mixing: A review and a model with a nonlocal boundary layer parameterization, Reviews of Geophysics, 32, 363–403, https://doi.org/10.1029/94RG01872, 1994.

Losch, M.: Modeling ice shelf cavities in az coordinate ocean general circulation model, Journal of Geophysical Research: Oceans, 113, 2008.

Love, K. B., Hallet, B., Pratt, T. L., and O'neel, S.: Observations and modeling of fjord sedimentation during the 30 year retreat of Columbia Glacier, AK, Journal of Glaciology, 62, 778–793, https://doi.org/10.1017/jog.2016.67, 2016.

MacCready, P.: Calculating Estuarine Exchange Flow Using Isohaline Coordinates, Journal of Physical Oceanography, 41, 1116–1124, https://doi.org/10.1175/2011JPO4517.1, 2011.

MacCready, P., Geyer, W. R., and Burchard, H.: Estuarine exchange flow is related to mixing through the salinity variance budget, Journal of Physical Oceanography, 48, 1375–1384, 2018.

MacCready, P., McCabe, R. M., Siedlecki, S. A., Lorenz, M., Giddings, S. N., Bos, J., Albertson, S., Banas, N. S., and Garnier, S.: Estuarine Circulation, Mixing, and Residence Times in the Salish Sea, Journal of Geophysical Research: Oceans, 126, e2020JC016 738, https://doi.org/https://doi.org/10.1029/2020JC016738, 2021.

Magorrian, S. J. and Wells, A. J.: Turbulent plumes from a glacier terminus melting in a stratified ocean, Journal of Geophysical Research: Oceans, 121, 4670–4696, https://doi.org/10.1002/2015JC011160, 2016.

Marshall, J., Adcroft, A., Hill, C., Perelman, L., and Heisey, C.: A finite-volume, incompressible Navier Stokes model for studies of the ocean on parallel computers, Journal of Geophysical Research: Oceans, 102, 5753–5766, 1997.

735 Moffat, C.: Wind-driven modulation of warm water supply to a proglacial fjord, Jorge Montt Glacier, Patagonia, Geophysical Research Letters, 41, 3943–3950, 2014.

Moffat, C., Tapia, F. J., Nittrouer, C. A., Hallet, B., Bown, F., Boldt Love, K., and Iturra, C.: Seasonal evolution of ocean heat supply and freshwater discharge from a rapidly retreating tidewater glacier: Jorge Montt, Patagonia, Journal of Geophysical Research: Oceans, 123, 4200–4223, 2018.

740 Mortensen, J., Lennert, K., Bendtsen, J., and Rysgaard, S.: Heat sources for glacial melt in a sub-Arctic fjord (Godthåbsfjord) in contact with the Greenland Ice Sheet, Journal of Geophysical Research: Oceans, 116, https://doi.org/10.1029/2010JC006528, 2011.

Mortensen, J., Bendtsen, J., Motyka, R. J., Lennert, K., Truffer, M., Fahnestock, M., and Rysgaard, S.: On the seasonal freshwater stratification in the proximity of fast-flowing tidewater outlet glaciers in a sub-Arctic sill fjord, Journal of Geophysical Research: Oceans, 118, 1382–1395, https://doi.org/10.1002/jgrc.20134, 2013.

745 Morton, B. R., Taylor, G. I., and Turner, J. S.: Turbulent gravitational convection from maintained and instantaneous sources, Proceedings of the Royal Society of London. Series A. Mathematical and Physical Sciences, 234, 1–23, https://doi.org/10.1098/rspa.1956.0011, 1956.

Motyka, R. J., Dryer, W. P., Amundson, J., Truffer, M., and Fahnestock, M.: Rapid submarine melting driven by subglacial discharge, LeConte Glacier, Alaska, Geophysical Research Letters, 40, 5153–5158, 2013.

Nilsson, J., van Dongen, E., Jakobsson, M., O'Regan, M., and Stranne, C.: Hydraulic suppression of basal glacier melt in sill fjords, The
750 Cryosphere, 17, 2455–2476, https://doi.org/10.5194/tc-17-2455-2023, 2023.

Rayson, M. D., Gross, E. S., Hetland, R. D., and Fringer, O. B.: Time scales in Galveston Bay: An unsteady estuary, Journal of Geophysical Research: Oceans, 121, 2268–2285, https://doi.org/https://doi.org/10.1002/2015JC011181, 2016.

Rignot, E., Fenty, I., Xu, Y., Cai, C., Velicogna, I., Cofaigh, C., Dowdeswell, J. A., Weinrebe, W., Catania, G., and Duncan, D.: Bathymetry data reveal glaciers vulnerable to ice-ocean interaction in Uummannaq and Vaigat glacial fjords, west Greenland, Geophysical Research
755 Letters, 43, 2667–2674, 2016.

Schaffer, J., Kanzow, T., von Appen, W.-J., von Albedyll, L., Arndt, J. E., and Roberts, D. H.: Bathymetry constrains ocean heat supply to Greenland's largest glacier tongue, Nature Geoscience, 13, 227–231, https://doi.org/10.1038/s41561-019-0529-x, 2020.

Sciascia, R., Cenedese, C., Nicolì, D., Heimbach, P., and Straneo, F.: Impact of periodic intermediary flows on submarine melting of a Greenland glacier, Journal of Geophysical Research: Oceans, 119, 7078–7098, https://doi.org/10.1002/2014JC009953, 2014.

760 Slater, D. A., Goldberg, D. N., Nienow, P. W., and Cowton, T. R.: Scalings for Submarine Melting at Tidewater Glaciers from Buoyant Plume Theory, Journal of Physical Oceanography, 46, 1839–1855, https://doi.org/10.1175/JPO-D-15-0132.1, 2016.

Straneo, F. and Cenedese, C.: The dynamics of Greenland's glacial fjords and their role in climate, Annual review of marine science, 7, 89–112, 2015.

Straneo, F., Hamilton, G. S., Sutherland, D. A., Stearns, L. A., Davidson, F., Hammill, M. O., Stenson, G. B., and Rosing-Asvid,
765 A.: Rapid circulation of warm subtropical waters in a major glacial fjord in East Greenland, Nature Geoscience, 3, 182–186, https://doi.org/10.1038/ngeo764, 2010.

Sutherland, D. A., Straneo, F., and Pickart, R. S.: Characteristics and dynamics of two major Greenland glacial fjords, Journal of Geophysical Research: Oceans, 119, 3767–3791, https://doi.org/10.1002/2013JC009786, 2014.

Wang, T., Geyer, W. R., and MacCready, P.: Total Exchange Flow, Entrainment, and Diffusive Salt Flux in Estuaries, Journal of Physical Oceanography, 47, 1205–1220, https://doi.org/10.1175/JPO-D-16-0258.1, 2017.

Xu, Y., Rignot, E., Menemenlis, D., and Koppes, M.: Numerical experiments on subaqueous melting of Greenland tidewater glaciers in response to ocean warming and enhanced subglacial discharge, Annals of Glaciology, 53, 229–234, 2012.

Xu, Y., Rignot, E., Fenty, I., Menemenlis, D., and Flexas, M. M.: Subaqueous melting of Store Glacier, west Greenland from three-dimensional, high-resolution numerical modeling and ocean observations, Geophysical Research Letters, 40, 4648–4653, https://doi.org/https://doi.org/10.1002/grl.50825, 2013.

Zhao, K. X., Stewart, A. L., and McWilliams, J. C.: Geometric Constraints on Glacial Fjord–Shelf Exchange, Journal of Physical Oceanography, 51, 1223–1246, 2021.
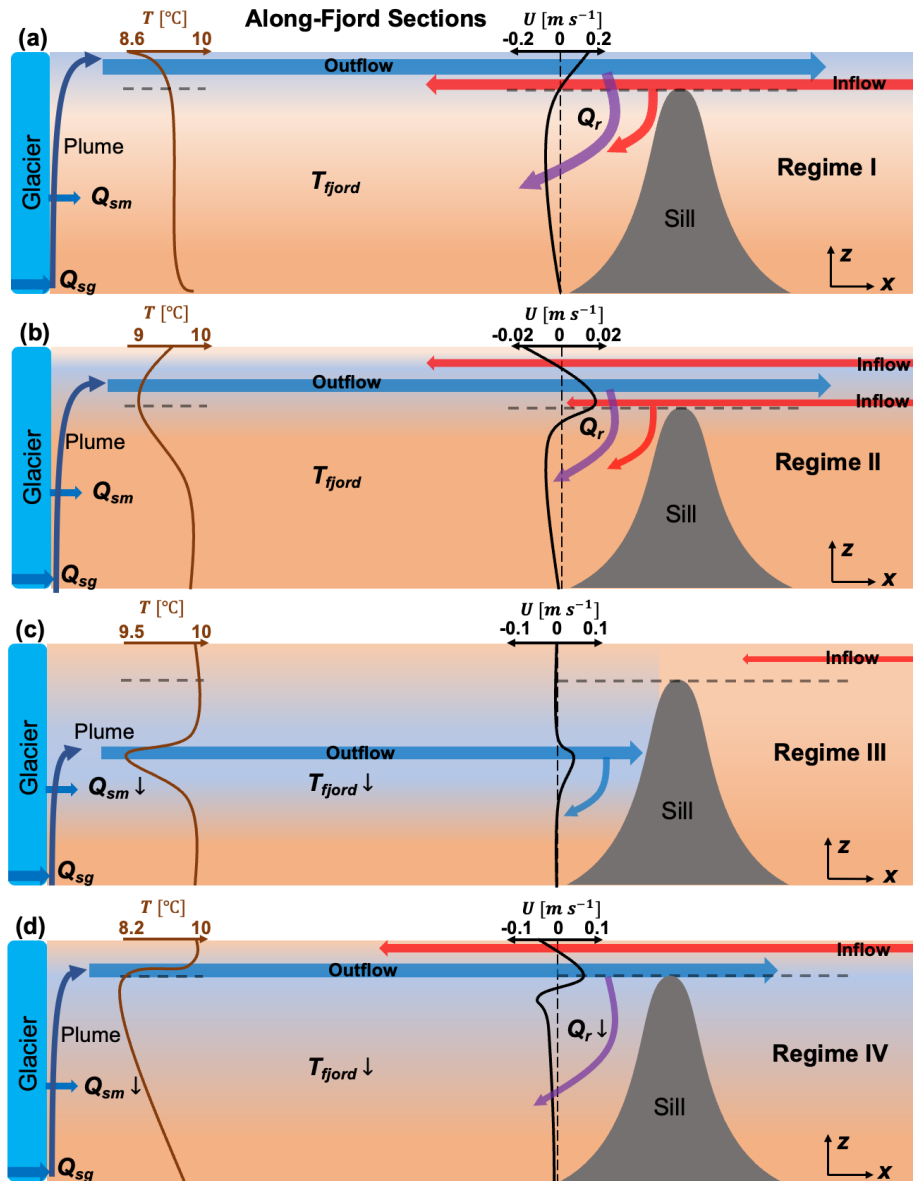
Figure 7. ~~Snapshots~~ Schematic of ~~fjord~~ circulation regimes ~~from side (left panel) and plan (right panel) views~~ in shallow-silled glacial fjords. ~~Black contours denote water density anomaly~~ Brown and black curves are approximate temperature profiles near the glacier front and along-fjord velocity profiles on the glacierward side of the sill, ~~white~~ respectively. Horizontal dashed gray lines indicate the ~~depths at which the plan-view snapshots are taken, grey shaded areas represent~~ maximum sill ~~locations~~ height. ~~Across-fjord structures~~ The colors of shades and arrows represent relative water temperatures. The sizes of the ~~regimes can be found in Fig~~ arrows indicate the relative magnitude of transports. ~~S1~~ Parameters depicted include subglacial discharge (Q_{sg}), submarine melting (Q_{sm}), deep-fjord temperature (T_s), and ~~Fig~~ sill-driven reflux (Q_r). ~~S2.~~

Figure 8. Snapshots of fjord circulation regimes from side (left panel) and plan (right panel) views. Black contours denote water density anomaly, white dashed lines indicate the depths at which the plan-view snapshots are taken, and gray-shaded areas represent sill locations. Across-fjord structures of the regimes can be found in Fig. S1 and Fig. S2.
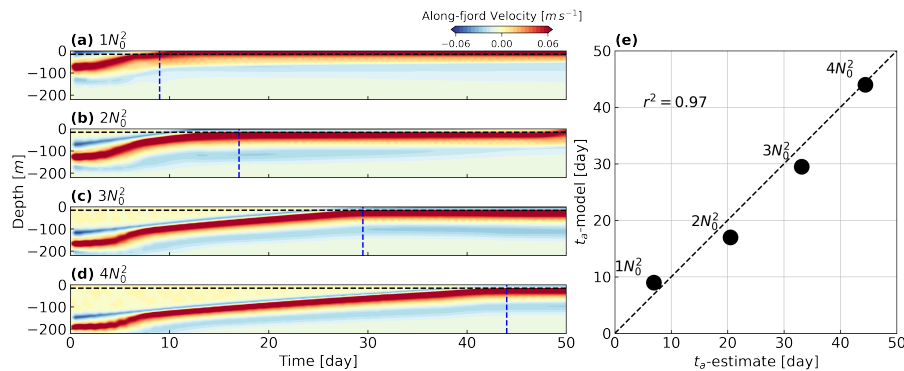
Figure 9. Ascending (t_a) of the plume with increasing initial stratification. (a)-(d): Evolution of the vertical structure of along-fjord velocity near the glacier front, with positive values toward the fjord mouth. Horizontal dashed black lines show the maximum sill height ($h_s/h_f = 0.04$), and vertical dashed blue lines indicate the estimated time for the plume rising from its initial height to the level of the sill crest. (e): A comparison between the plume ascending time estimated from theory and the model output.
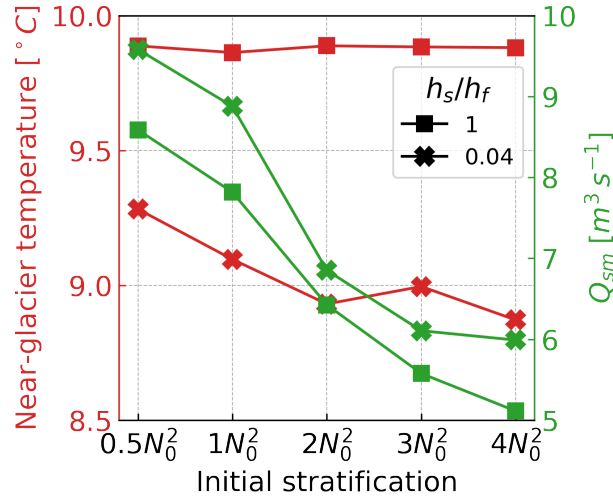
Figure 10. Impact of shallow sill vs. fjord stratification on near-glacier temperature and submarine melting, results are averaged over the last 14 days of each simulation.
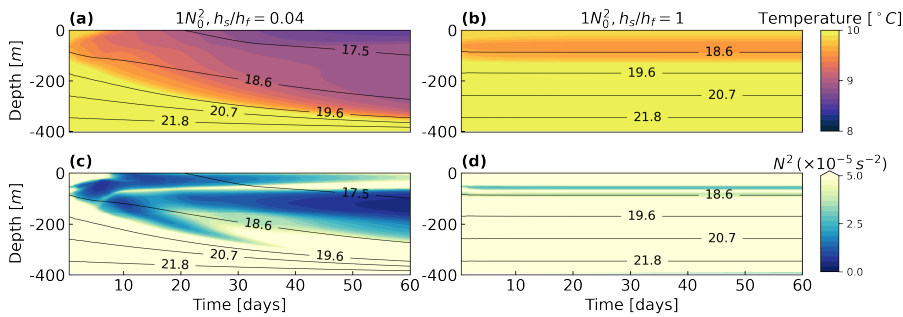
~~Schematics of fjord structure and circulation for different regimes. Brown and black curves are approximate temperature profiles near the glacier front and along-fjord velocity profiles on the glacierward side of the sill respectively. Horizontal dashed grey lines indicate the maximum sill height. Colors of shades and arrows represent relative water temperatures. Sizes of arrows indicate the relative magnitude of transports. Parameters depicted include subglacial discharge (Q_{sg}), submarine melting (Q_{sm}), deep-fjord temperature (T_s), and sill-driven reflux (Q_r).~~

Figure 11. The evolution of near-glacier temperature (a, b), and near-glacier stratification (c, d) at S0 (near the glacier) with (left panel) and without (right panel) a sill. Forcing and initial conditions other than the sill depth are the same.
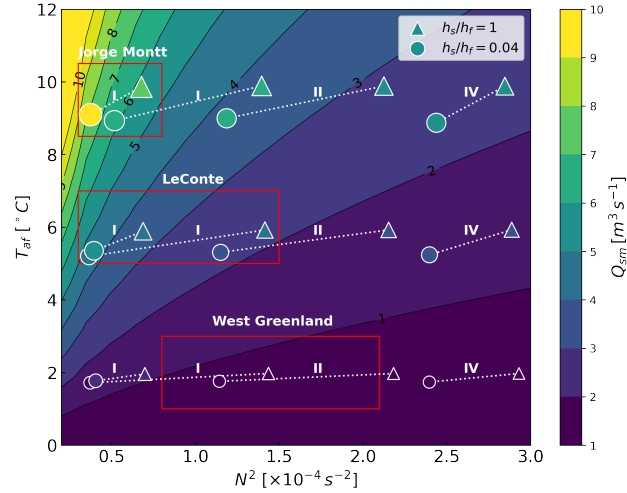
Figure 12. Dependence of submarine melt on fjord stratification and thermal forcing with a constant subglacial discharge of $Q_{sg} = 250 \, m^3 \, s^{-1}$. Cases with the same initial temperature ($2°C$, $6°C$, $10°C$) and stratification ($1N_0^2, 2N_0^2, 3N_0^2, 4N_0^2$) but no or shallow sill are connected by white dotted lines. The sizes and colors of the markers represent the magnitude of Q_{sm} for each run. The background contours correspond to the scaling of Q_{sm} based on $(T_{af})(N^2)^{-5/8}$ with an added proportionality constant calculated from the model output (Fig. S6). The results are averaged over the last 14 days of each simulation, corresponding to circulation regimes determined by initial stratification ($1N_0^2 \& 2N_0^2$: Regime I, $3N_0^2$: Regime II, $4N_0^2$: Regime IV). The red boxes highlight approximate observed ranges of glacial fjord properties from Patagonia (Jorge Montt; Moffat et al., 2018), Alaska (LeConte; Jackson et al., 2022), and West Greenland (e.g., Mortensen et al., 2011; Gladish et al., 2015).